REVIEW ARTICLE

Pollutants degradation and power generation by photocatalytic fuel cells: A comprehensive review

Yasser Vasseghian [a], Alireza Khataee [a,b], Elena-Niculina Dragoi [c], Masoud Moradi [d,**], Samaneh Nabavifard [e], Gea Oliveri Conti [f], Amin Mousavi Khaneghah [g,*]

[a] Institute of Research and Development, Duy Tan University, Da Nang 550000, Vietnam
[b] Research Laboratory of Advanced Water and Wastewater Treatment Processes, Department of Applied Chemistry, Faculty of Chemistry, University of Tabriz, 51666-16471 Tabriz, Iran
[c] Faculty of Chemical Engineering and Environmental Protection "Cristofor Simionescu", "Gheorghe Asachi" Technical University, Iasi, Bld Mangeron No 73, 700050, Romania
[d] Research Center for Environmental Determinants of Health (RCEDH), Health Institute, Kermanshah University of Medical Sciences, Kermanshah, Iran
[e] Police Sciences and Social Studies Institute, Tehran, Iran
[f] Environmental and Food Hygiene Laboratories (LIAA), Department of Medical, Surgical Sciences and Advanced Technologies "G.F. Ingrassia", Hygiene and Public Health, University of Catania, Via S. Sofia 87, 95123 Catania, Italy
[g] Department of Food Science, Faculty of Food Engineering, State University of Campinas (UNICAMP), 13083-862 Campinas, São Paulo, Brazil

Abstract Wastewater contains organic compounds (fatty acids, amino acids, and carbohydrates) that have a significant amount of chemical energy. In this regard, the use of wastewater for recovering energy by some appropriate energy conversion technologies can be considered as an appropriate approach to simultaneously achieve the reduction of environmental contamination and increasing supply of energy. The Photocatalytic Fuel Cell (PFC) can provide a new approach in developing technology for simultaneous organic pollutants removal from wastewaters and power generation, but it also has disadvantages, such as requires higher voltage, more cost and complexity. To present a comprehensive vision of the current state of the art, and progress the treatment effi-

* Corresponding author.
** Co-corresponding author.
 E-mail addresses: mahfooz60@gamil.com (M. Moradi), mousavi@unicamp.br (A. Mousavi Khaneghah).
Peer review under responsibility of King Saud University.

Production and hosting by Elsevier

ciency and agitate new studies in these fields, this review discussed the study covering PFC aspects, with a focus on the comparison of pollutant degradation, power generation, different photoanode and photocathode materials as well as the application of the Fenton process in PFCs.
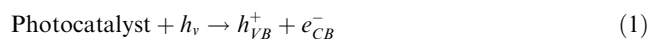
1. Introduction

Conventional water and wastewater treatment processes are not effective in removing and/or degrading a number of pollutants, as well as, some efficient treatment techniques e.g. reverse osmosis (RO) usually require high energy consumption for purification (for example, 5–100 kwh/kgCOD) (Li et al., 2019). An efficient solution to overcome this challenge is to add an additional unit of advanced oxidation processes (AOPs) to conventional water treatment equipment (Liu et al., 2019; Liu et al., 2017). AOPs are widely used to decompose several organic substances to highly reactive chemicals (Khatri et al., 2018; Vasseghian and Dragoi, 2018; Vasseghian et al., 2020). Among them, semiconductor-based photocatalytic processes have been widely welcomed as an efficient option due to their eligible properties such as high efficiency, low cost, high stability, low toxicity and chemical inertness (Sarac et al., 2020; Wang et al., 2019). The low level of rich chemical energy obtained during the process of elimination from organic decomposition is one of the main disadvantages of most AOPs (Jiang et al., 2018; Pirsaheb et al., 2019; Wang et al., 2019). On the other hand, the organic compounds in sewerage can be used as sources of carbon and energy that can be applied. Thus, It is essential to extend sustainable methods that can degrade these organic contaminants and synchronous recover their chemical energy (Li et al., 2019; Li et al., 2017). The Photocatalytic Fuel Cell (PFC) is a successful scheme for wastewater treatment and synchronous recovery of chemical energy from the wastewater (Lee et al., 2018). The non-selective properties of the photocatalyst lead to the degradation of an extensive range of pollutants such as dyes (Nordin et al., 2019; Lee et al., 2018; Ong et al., 2019; Khalik et al., 2017; Tang et al., 2019), antibiotics (Li et al., 2019; Zhao et al., 2017; Deng et al., 2018; Lu et al., 2019), heavy metal ions (Wang et al., 2017), alcoholic compounds (Xia et al., 2016; Sfaelou et al., 2014). However, a high similarity between PFC and other fuel cells (FC) types (such as microbial FC-MFC- (Fang et al., 2016); direct methanol FC (Wu et al., 2017), proton exchange membrane FC (Qi et al., 2018); alkaline polymer electrolyte membrane FC (Lan et al., 2015), can be observed. While this technique is able to simultaneously degrade organic pollutants from the wastewater and produce power (Khalik et al., 2017).

Compared to conventional MFCs, PFCs have the following desirable features, but may not be limited to: (i) PFC can use sunlight as an energy source and lead to the fast generation and direct transfer of electrons, thus increasing the degradation efficiency of pollutants; (ii) It is possible to design high-performance electromaterials for PFC by nanotechnology; (iii) PFC can be easily fabricated and operated in finite reaction conditions by controlling the light input; and (iv) PFC system has strong oxidative ability of photogenerated holes and

•OH by non-selective oxidation of substrates (Li et al., 2019; Kee et al., 2018).

The PFC needs a photoanode carrying photocatalyst and light radiation (LR) to generate electrons (e^-) to decompose organic pollutants and generate power (Eq. (1)). In order to ensure that the e^- are excited in the conduction band (CB) and that they can leave the holes (h^+) in the valence band (VB), the radiation energy should be higher or equal to the photocatalyst energy band. The UV irradiation of the anode detaches the photogenerated e^- and h^+ (Eqs. (2) and (3)). For power generation, due to the organic compounds' decomposition in the anode, e^- are provided and transmitted to the cathode by means of an external circuit (Eq. (4)). The hydrogen ions generated by the photooxidation process are transferred to the cathode by diffusion using a proton exchange membrane (PEM). Oxygen is provided at the cathode and the transferred e^- react with O_2, thus resulting in water (Eqs. (5)–(10)) or superoxide radicals (Eqs. (12) and (13)) (Lee et al., 2018).

Photoexcitation of photocatalyst:

$$Photocatalyst + h_v \rightarrow h_{VB}^+ + e_{CB}^- \tag{1}$$

Generation of •OH

$$h_{VB}^+ + OH^-(ads) \rightarrow OH \tag{2}$$

$$h_{VB}^+ + H_2O \rightarrow OH + H^+ \tag{3}$$

Redox reactions

$$h_{VB}^+ + Organics \rightarrow Organics^+(oxidation\ of\ organics) \tag{4}$$

$$OH + Organics \rightarrow Organics (degradation\ of\ organics) \tag{5}$$

$$Organics + O_2 \rightarrow Organics - OO (degradation\ of\ organics) \tag{6}$$

$$\cdot O_2^- + Organics \rightarrow Organics - OO (degradation\ of\ organics) \tag{7}$$

$$e^- + Organics \rightarrow Organics (reduction\ of\ organics) \tag{8}$$

$$Organics^+ \rightarrow Organics^{2+} + e_{CB}^-(injection\ of\ electron\ in\ the\ CB) \tag{9}$$

$$4H^+ + O_2 + 4e^- \rightarrow 2H_2O \tag{10}$$

$$2H_2O + 2H^+ + 2e^- \rightarrow H_2O_2 \tag{11}$$
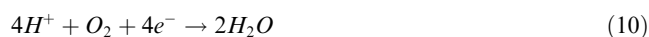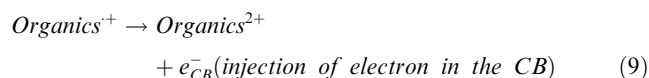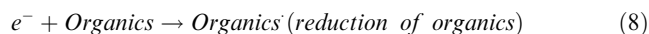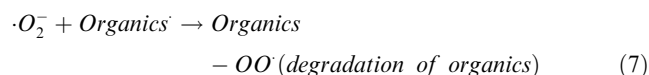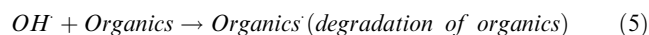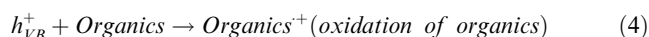
Generation of superoxides:

$$e_{CB}^- + O_2 \rightarrow \cdot O_2^- \tag{12}$$

$$e^- + O_2 \rightarrow \cdot O_2^-(reaction\ at\ the\ cathode) \tag{13}$$

Significantly, most species of PFC reactions occur mainly on the surfaces of the electrodes. Additionally, in the solution, the reaction time is limited by the partly mass transfer and thus, the processing time is delayed. Consequently, in order to raise the efficiency of reactivity of materials and improve the mass transfer in the liquid phase, the PFC is commonly used in combination with materials such as carbon nanotubes (Das et al., 2017); graphene (Xiang et al., 2012) and metal oxides (Martin et al., 2015). TiO_2, as one of the most important photocatalytic materials, is mainly employed due to high stability (physical and chemical) and unique properties (optical and electronic), easy to prepare, low cost and non-toxic (Li et al., 2014; Khataee et al., 2014). However, the fast recombination e_{CB}^- and h^+ in TiO_2 reduces the efficiency of photocatalytic degradation (Mousavi et al., 2020; Ying et al., 2016). In this regard, some new anodes have been introduced to raise the absorption capacity of radiation and e^--h^+ separation on the photoelectrode surface (Table 1).

In this context, an overview of photocatalytic fuel cells for the degradation of pollutants and simultaneous power generation is presented. The effect of different photoanode and photocathode materials on pollutant degradation and power generation were discussed. To better understand the Fenton process on photocatalytic fuel cell systems, an analysis regarding the hybrid system of Fenton process and photocatalytic fuel cell for pollutant degradation and power generation was also performed.

2. Pollutant degradation

The water pollution crisis is one of the environmental problems generated by the development among human' life. Discharging wastewater with organic pollutants such as dye (Iqbal et al., 2017; Mousavi et al., 2020; Xie et al., 2012; Yang et al., 2018) and antibiotics (Hailili et al., 2018; Osouleddini et al., 2019) are the most important segments of water pollution (Zarei et al., 2012). In this regard, recently some effective technologies were employed to reduce the toxic wastewater issue (Liu et al., 2016; Alikarami et al., 2019; Khataee et al., 2011). Among them, the PFC system has recently been approached as a promising technology to treat a wide range of colored wastewater (Katsumata et al., 2013).
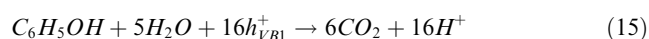
Based on the PFC mechanism (Eqs. (1)–(13)), when the photoanode is irradiated by light, the e^- are excited from VB into the CB (Eq. (1)). The band gap is also known as an energy gap and it will be further referred to as Eg. Then, it could react with the hydroxide ions or water molecules to produce the OH^- (Eqs. (2) and (3)). Afterward, azo bonds are oxidized: i) directly, by photogenerated h^+ (Eq. (4)); or ii) indirectly, by OH^- (Eq. (5)). The e^- move to the cathode and react with the hydrogen ions produced through photooxidation to water (Eq. (10)). In this process, the HO and O_2^- leads to photocatalytic degradation of organic contaminants (Fig. 1).

In the case of Methylene Blue (MB) degradation, Chen et al. utilized an aerated PFC with nanopore WO_3/W photoanode and a Pt modified commercial silicon photovoltaic cell (Pt/PVC) photocathode (Chen et al., 2014). They were able to remove 14% of MB under the photolysis condition after 90 min and 91% of MB under aerated condition after 60 min. The Fermi level discrepancy between the two elec-

trodes can make the e^- to immigrate from photoanode to photocathode. Under aeration condition, the O_2 molecules use the e^- of Pt/PVC photocathode. To produce stable electricity in the external circuit, the h^+ of Pt/PVC can catch the e^- from WO_3/W. Therefore, the WO_3/W h^+ can be generated by pollutants decomposition. According to the mentioned phenomena, in this system, the simultaneous recovery of energy and organic pollutant degradation can occur (Chen et al., 2014).

Tang et al. (Tang et al., 2014) (Tang et al., 2014) used a rotating disk PFC (RDPFC) that has as photoanode a TiO_2/Ti disk. The system degrades RhB and Reactive Brilliant Red X-3B (RBR X-3B) and is formed by a Pt black/Pt cathode, NaOH anolyte, and H_2SO_4 catholyte. The proposed system had promising results, being practical to generate electricity and hydrogen (H_2) energy under UV lighting and different types of dye wastewater. As the enhancement of dye concentration leads to a significant decrease of sample solution transmittance, the sample solution in the immersion reactor absorbs a high percentage of the ultraviolet light, thus leading to a low degradation efficiency; on the other hand, LR absorption by solution significantly decreased in the aqueous film RDPFC and retained efficiency with sensible performance and promising performance.

In another study, Wu et al. (Wu et al., 2015) (Wu et al., 2015) investigated the phenol removal efficiency using a PFC with TiO_2 NRs/FTO photoanode, and C/Cu_2O NWAs/Cu mesh photocathode. The system displays a remarkable performance for the degradation of phenol so that 84.2% TOC removal was achieved in 8 h. The reaction process in this study can be explained by Eqs. (14)–(18) (Wu et al., 2015). Moreover, the photoresponse of the photocatalyst and conductivity of the substrates can affect the PFC performance in pollutant degradation. Results indicated short circuit current (J_{SC}) of TiO_2 NRs/FTO PFC is far more than Jsc of TiO_2 NTs/Ti PFC. The high value of J_{SC} showed the PFC system has a synergistic facilitated impact on the photoresponse of the photoanode and photocathode. The Fermi level of TiO_2NRs/FTO is further negative than that of C/Cu_2O NWAs/Cu mesh, resulting in a self-driven PFC during solar LR. For this system, the residual photoanode h^+ and the photocathode e^- lead to simultaneous organic compound degradation and H_2 generation (Xie et al., 2017).

$$TiO_2 + h_v \rightarrow h_{VB1}^+ + e_{CB1}^- \tag{14}$$

$$C_6H_5OH + 5H_2O + 16h_{VB1}^+ \rightarrow 6CO_2 + 16H^+ \tag{15}$$

$$Cu_2O + h_v \rightarrow h_{VB2}^+ + e_{CB2}^- \tag{16}$$

$$e_{CB}^- + h_{VB2}^+ \rightarrow h_v' \tag{17}$$

$$2H^+ + 2e_{CB2}^- \rightarrow H_2 \tag{18}$$

Also, Yang et al. (Yang et al., 2015) (Yang et al., 2015) applied a dual-chamber rotating-disk PFC with TiO_2 nanotube array/Ti (TNA/Ti) rotating-disk photoanode and Cu rotating-disk cathode for degradation RhB, RBR X-3B, MB, Bisphenol A (BPA), and Glucose. They succeeded to remove 96.8%, 69.8%, 92.9%, 86.9% and 93.2% of RhB, RBR X-3B, MB, Glucose, and RhB/BPA in anode chamber and 89.8%, 50.9%, 84.7%, 54.8% and 71.3% of RhB, RBR X-3B, MB, Glucose, and RhB/BPA in cathode chamber, respectively.
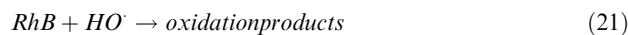
Table 1 Characteristics of some PFC that have been employed in recent years.

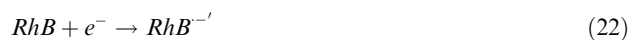| Authors/Year	Type of anodes	Characteristics of the PFCs	Substrates	Light source	Maximum power density (P_{max}, W m^{-2})	Type of electrolyte	Effective photo-electrodes surface area (cm^2)	Refs.
Antoniadou et al./2011	CdS/ZnS/TiO$_2$	PFC was manufactured from two rectangular compartments, filled with aerated electrolyte and separated by a silica frit. Both compartments included the same. UVA agitation of the anode was done by Black Light fluorescent tubes. An array of parallel tubes (each of 4 W nominal power) was set in front of the cell window, generating around 4.0 mW/cm^2 of light on the titania film. The excitation was generated by a Xe lamp that simulated solar radiation. In all cases, glass-FTO electrode as a window passes the exciting irradiation through itself.	–	Ultraviolet A (UVA)	–	NaOH	0.5	(Antoniadou et al., 2011)
Liu et al. / 2016	Ag/AgCl/GO	The PFC system had two photo-electrodes, a LED lamp (2 W) as a visible light source and an irradiation surface of 20 mm × 50 mm. The cell in a quartz tube (30 mm × 18 cm) had an aeration device, Ag/AgCl/GO-based anode and ZnIn$_2$S$_4$-based cathode placed at 2.5 cm from one-another. When the system was running, a 1 U resistance connected the anode.	Rhodamine B	Visible light	0.540	Na$_2$SO$_4$	-	(Liu et al., 2016)
Xie and Ouyang/2017	WO$_3$/FTO	The 2 × 2 cm^2 WO$_3$/FTO anode with an effective area of 3.0 cm^2 was fixed by an electrode holder and collected with the air-breathing cathode (3.0 cm diameter and 7.1 cm^2 effective area) through copper wire. The distance between the anode and cathode was ∼ 2 cm. The Pt/C catalyst loaded side of the air-breathing cathode was in direct contact with the electrolyte and the other side (without the catalyst) was exposed to air.	Oxytetracycline hydrochloride	Simulated solar light	0.363	Na$_2$SO$_4$	3.0 (anode), 7.1 (cathode)	(Xie and Ouyang, 2017)
Lee et al./2017	ZnO/Zn	The system had an immobilized ZnO/Zn anode and a Pt/C cathode, placed at 5 cm from each other. An ultraviolet A (UVA) lamp was place at 15 cm from the anode represented the light source. Aeration was supplied at the cathode side.	Reactive Green 19	Ultraviolet A (UVA)	0.102	Without adding any supporting electrolyte	15	(Lee et al., 2017)
Xie et al./2017	ZnFe$_2$O$_4$/TiO$_2$-NTs	The system has 2 × 2 cm^2 ZnFe$_2$O$_4$/TiO$_2$-NTs anode (3.0 cm^2 effective area) and an air-breathing cathode (3.0 cm diameter and 7.1 cm^2 effective area) placed at ∼2 cm from each other. An electrode holder fixed the anode that was connected with the air-breathing cathode using copper wire. The Pt/C catalyst side of the air-breathing cathode was in direct contact with the electrolyte and the other side was exposed to the air (to receive oxygen from the surrounding environment). A 300 W Xe lamp with an AM 1.5 filter simulated the solar light.	Phenolic compounds and pharmaceutical products	Simulated solar light	0.013	Na$_2$SO$_4$	3.0 (anode), 7.1 (cathode)	(Xie et al., 2017)
Zeng et al. / 2018	TiO$_2$/WO$_3$/W	The PFC was constructed using a dual-electrode configuration. The PFC was equipped an AM 1.5 illumination and 1 cm^2 illumination area for both the WO$_3$/TiO$_2$ anode and Pt/BJS cathode.	Atrazine	Visible light	0.563	K$_2$SO$_4$	–	(Zeng et al., 2018)

Table 1 (continued)

Authors/Year	Type of anodes	Characteristics of the PFCs	Substrates	Light source	Maximum power density (P_{max}, W m^{-2})	Type of electrolyte	Effective photo-electrodes surface area (cm^2)	Refs.
Ye et al. / 2018	TiO$_2$ nanotube array (TNA)	The system had a TNA electrode (3 cm × 3 cm) as photoactive anode and a copper foil (Grade M2, 3 cm × 4.5 cm) as counter electrode placed at 2 cm from each other. The reaction cell (6 cm × 6 cm × 6 cm) is a rectangular quartz cube. A 450 mW UV-LED lamp (365 nm peak intensity) placed outside the reaction cell (on the side of TNA anode) generated 11.6 mW/cm^2 radiant power at the TNA surface.	Micropollutant 4-chloro-2-methylphenoxyacetic acid	UV	–	Na$_2$SO$_4$	9.0	(Ye et al., 2018)
Ong et al. / 2019	ZnO/BaTiO$_3$	An anode and platinum-loaded carbon (Pt/C) cathode (connected by a 1 kΩ resistivity external circuit) were placed in a 1000 ml Pyrex glass cell filled with 500 ml of RR120. Two ultraviolet A (UVA) lamps (placed at 100 mm from the anode and cathode) were used as the light source.	Reactive Red 120	Ultraviolet A (UVA)	0.005284	Without adding any supporting electrolyte	–	(Ong et al., 2019)

The results revealed that the organic degradation process can be done in both the anode and cathode chamber with different pathway. Under UV irradiation the hole could be generated in the anode which leads to direct oxidation of the pollutant, Eqs. (19)–(21).

$$RhB + h_{VB}^+ \rightarrow RhB^{\cdot +'} \tag{19}$$

$$h_{VB}^+ + H_2O \rightarrow HO^{\cdot} \tag{20}$$

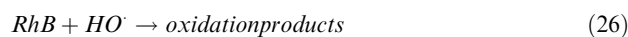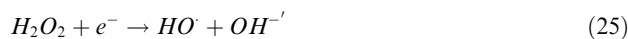$$RhB + HO^{\cdot} \rightarrow oxidation products \tag{21}$$

While both direct and indirect processes are involved in the pollutant degradation by cathode chamber as depicted in the following equations:
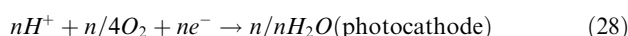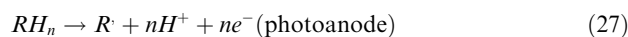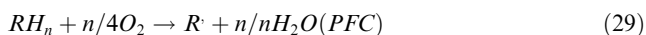
Direct pathway:

$$RhB + e^- \rightarrow RhB^{\cdot -'} \tag{22}$$

Indirect pathway:

$$O_2 + 2H^+ + e^- \rightarrow H_2O_2 \tag{23}$$

$$RhB + H_2O_2 \rightarrow oxiation products \tag{24}$$

$$H_2O_2 + e^- \rightarrow HO^{\cdot} + OH^{-'} \tag{25}$$

$$RhB + HO^{\cdot} \rightarrow oxidation products \tag{26}$$

To decompose the existing organic pollutants from water samples, the organic compounds represented the source of energy. It has a series of advantages that include: i) increased efficiency of LR utilization attained by a thin-film photocatalytic reaction and TNA photoanode; ii) more suitable $h^+ - e^-$ separation through the TNA microstructure; iii) enhanced mass transfer via electrodes rotation; and iv) in situ production of H$_2$O$_2$ and •OH (that simplifies the decomposition of organic compounds). The appropriate efficiency was ascribed to various decomposition pathways such as direct e^- reduction, direct h^+ oxidation, indirect •OH oxidation, and indirect H$_2$O$_2$ oxidation. The e^- migration could produce usable electricity, a fact that represents an advantage over conventional PFCs (Zeng et al., 2018).

Bai et al. (Bai et al., 2016) (Ye et al., 2018) investigated Methyl Orange (MO), CR and MB removal efficiency by a PFC with BiVO$_4$/TiO$_2$nano-tubes/FTO photoanode and ZnO/CuO nanowires/FTO photocathode. They achieved to remove 76%, 83%, and 90% of MO, CR, and MB, respectively. The mechanism of pollutants degradation is due to this fact that the Fermi level of BiVO$_4$/TiO$_2$ is far more negative than ZnO/CuO which leads to migration of the he BiVO$_4$/TiO$_2$ e^- and the ZnO/CuO h^+ can be moved by an internal bias and then discharged to simultaneously recover energy and decompose organic compounds. On the other hand however, the photocathode electrons and photoanode holes would be released and contribute to the organic pollutants (Eqs. (27)–(29)). Moreover, the type of substrate affects the PFC performance so that PFC performed better in the presence of phenol and glucose. This can correspond to differences in the molecular structure of organic matter (Bai et al., 2016).

$$RH_n \rightarrow R^{\cdot} + nH^+ + ne^- \, (\text{photoanode}) \tag{27}$$

$$nH^+ + n/4O_2 + ne^- \rightarrow n/nH_2O \, (\text{photocathode}) \tag{28}$$

$$RH_n + n/4O_2 \rightarrow R^. + n/nH_2O(PFC) \tag{29}$$

Furthermore, for the Reactive Green 19 (RG19) degradation, Lee et al. employed a PFC having a ZnO/Zn photoanode and platinum loaded carbon cathode. In this study, the effect of several inert electrolytes such as NaCl, Na$_2$SO$_4$, and MgSO$_4$, aeration, and initial concentration of dye on performance was investigated. It was shown that NaCl inert electrolyte has the highest RG19 degradation efficiency (100% after 8 h) due to the direct reaction of NaCl with $^\bullet$OH generated on the surface of the ZnO Photoanode. On the other hand, hypochlorite ions could be produced from NaCl solution (Eqs. (30)–(32)) which leads to indirect oxidation of RG19 (Lee et al., 2016).

$$2Cl^- \rightarrow Cl_2 + 2e^- \tag{30}$$

$$Cl_2 + H_2O \rightarrow HOCl + H^+ + Cl^- + \tag{31}$$

$$HOCl \rightarrow H^+ + Cl^- \tag{32}$$

The addition of Na$_2$SO$_4$, NaCl, and MgSO$_4$ as inert electrolytes lead to a high Jsc and Pmax. This can be explained by the fact that the conductivity of the media enhanced with the inert electrolyte leads to a decreased PFC internal resistance. Furthermore, the existence of chloride ions contributes to a direct, strong oxidation reaction at the anode surface that, as a result, enhances degradation. For MgSO$_4$ and Na$_2$SO$_4$, due to the absence of chloride, the degradation rates were not as good as that of NaCl. Totally, the presence of supporting electrolyte significantly enhances the removal of color. Because the electrolyte causes increased the potential difference on the electrodes. This phenomenon facilitates the spontaneous flow of photogenerated electrons to the cathode and subsequent generation of oxidizing photogenerated holes in the valence band of the anode (Shen et al., 2006).

Initial concentration of the pollutant is the other factor that affects the PFC performance. The removal efficiency of RG19 was decreased with increasing of RG19 up to 30 mg/L. This due to prevent of UV transmission from the solution to the photoanode which leads to restricted availability of photon for $^\bullet$OH generation. On the other hand, the photoexcitation of photoanode can be decreased with increasing of initial concentration of RG19 (Saquib and Muneer, 2003; Saquib and Muneer, 2003).

RhB removal was also studied by Sui et al. (Sui et al., 2017), as a PFC equipped with a biocathode and TiO$_2$ and Ag/TiO$_2$ photoanodes was used. The anode was designed by doping Ag into the three-dimensional TiO$_2$ nanoarrays formed on Ti mesh. A 99.5% removal rate was obtained with Ag/TiO$_2$ photoanode and 97.3% with TiO$_2$ photoanode. For both types of photoanode, the RhB removal followed pseudo-first-order kinetics. The photoanode made of Ag/TiO$_2$ is significantly better (in terms of RhB decomposition and electricity production performance) than that made of TiO$_2$.

After 90 min operation, Zhao et al. (Zhao et al., 2017) reported a removal rate of 91.98%, 98.57%, 92.36% and 68.09% for MO, MB, CR and Tetracycline (TC), respectively using a hybrid Fenton-PFC system with TiO$_2$ TNA photoanode and the Pt/SiPVC photocathode. The degradation efficiency for these compounds in traditional PFC (without ferrous ions) was 53.61%, 45.38%, 51.09%, and 30.65%, respectively. The main reason for this increase can be corre-
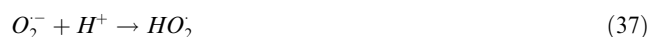
lated with the introduction of Fe^{2+} to the system which leads to an intensification of radical reactions and thus, the degradation efficiency increases (more details about this issue are provided in section 7).

Also, Zhao et al. (2017) (Zhao et al., 2017) proposed a system that increases organic decomposition and electricity generation concurrently by using Fe^{2+} ions to intensify the reaction of radicals. The system had TiO$_2$ TNA photoanode and Pt-black/Pt photocathode and was used for degradation of MO, MB, Congo Red (CR), and TC. The degradation efficiency for MO, MB, CR, and TC in traditional PFC was 34.99%, 43.75%, 40.58%, and 34.40%, respectively, but after adding the ferrous ions to the system, the degradation efficiency for these compounds increased to 97.34%, 95.36%, 93.23%, and 73.80%, respectively. In addition, the process parameters (pH, electrolyte, Fe^{2+} concentration) were evaluated.

The mechanism of pollutant degradation is assigned to hydroxyl radical via electron-hole pairs are generation during UV irradiation as presented in the Eqs. (33) and (34).

$$TiO_2 + h\vartheta \rightarrow h^+ + e^- \tag{33}$$

$$H_2O + h^+ \rightarrow HO^. + H^+ \tag{34}$$

On the other hand, continuous current in the cathode leads to electrons reducing O$_2$ which causes the generation of different reactive radicals Eqs. (35)–(38).

$$O_2 + e^- \rightarrow O_2^{.-} \tag{35}$$

$$O_2 + 2H^+ + 2e^- \rightarrow H_2O_2 \tag{36}$$

$$O_2^{.-} + H^+ \rightarrow HO_2 \tag{37}$$

$$HO^. + H_2O_2 \rightarrow HO_2^. + H_2O \tag{38}$$

Also, the electrolyte concentration influence the PFC performance, so that increasing of sodium sulfate concentration from 0.00 mol/L to 0.10 mol/L cause the enhancement of color removal from 58.47% to 97.34%. This due to increasing of solution conductivity which leads to transmitted of photoinduced e$^-$ through the external circuit of the PFC (Zhao et al., 2017).

To remove RG19, Lee et al. (2018) (Lee et al., 2018) applied a membrane-less PFC with a photoanode made of ZnO loaded carbon and a cathode made of Pt loaded carbon. The effect of dissolved oxygen (DO) was investigated on the degradation efficiency and it was shown that because the DO maintains the e$^-$- h$^+$ pair separation of ZnO, the DO concentration increase leads to a rise of RG19 removal rate. It was also shown that the decolorization performance is 37% at a slow rate (k = 0.033 h^{-1}), low DO concentration (roughly 0.2 mg L^{-1}), and N$_2$ gas for 8 h. Moreover, the e$^-$, h$^+$, $^\bullet$OH, O$_2^{\bullet-}$, OO$^\bullet$ and H$_2$O$_2$ are the main radicals which contribute in the dye degradation process (Eqs. (1)–(13)).

In another study, Li et al. (Li et al., 2018) applied a PFC coupling with persulfate (PS) activation TiO$_2$ nanotube arrays on a titanium sheet as the photoanode to remove MO. The proposed system could enhance the reaction of photocatalytic MO removal using the formation of active species (SO$_4^{\bullet-}$ and $^\bullet$OH) from the solid electrodes surface to the total liquid phase. For this reason, PFC/PS represented significant cell efficiency, raising the MO degradation by 40.36% (compared to PFC without PS), reaching 90.19%. Furthermore, the MO
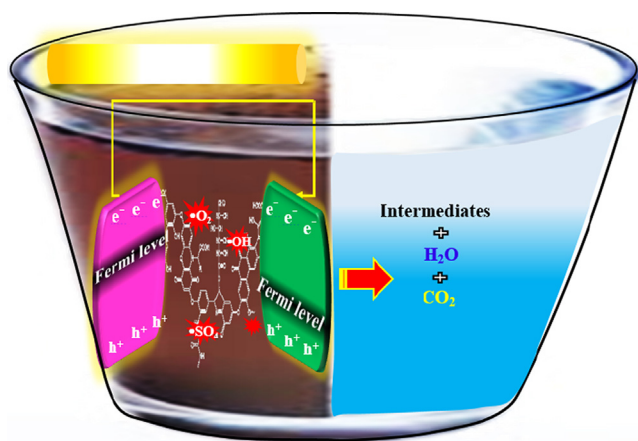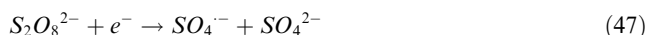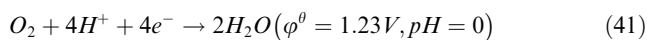
Fig. 1 Schematic of pollutants degradation in PFC.

degradation process conforms the pseudo-first-order kinetics model, the removal mechanism being described by Eqs. (39)–(47). In this connecting system, electricity production was higher by 44.97% than the bare PFC (Li et al., 2018).

$$TiO_2 + h_v \rightarrow h^+ + e^- \tag{39}$$

$$H_2O_2 + h^+ \rightarrow OH + H^+ \tag{40}$$

$$O_2 + 4H^+ + 4e^- \rightarrow 2H_2O \left(\varphi^\theta = 1.23V, pH = 0 \right) \tag{41}$$

$$O_2 + e^- \rightarrow \cdot O_2^- \tag{42}$$

$$O_2 + 2H^+ + 2e^- \rightarrow H_2O_2 \tag{43}$$

$$\cdot O_2^- + H^+ \rightarrow H_2O \tag{44}$$

$$HO \cdot + H_2O_2 \rightarrow HO_2 \cdot + H_2O \tag{45}$$

$$S_2O_8^{2-} + h_v \rightarrow 2SO_4 \cdot^- \tag{46}$$

$$S_2O_8^{2-} + e^- \rightarrow SO_4 \cdot^- + SO_4^{2-} \tag{47}$$

In another study, Lu et al. (Lu et al., 2018) (Lu et al., 2018) applied a PFC with $BiOBr/TiO_2$ TNAs with 5, 10, 15, and 20 consecutive ionic layer adsorption and reaction cycles photoanode and Pt cathode for RhB removal. Using this system, 99.7% of RhB was removed; the working mechanism is described by Eqs. (48)–(49) at the photoanode and Eqs. (50)–(51) at the photocathode.
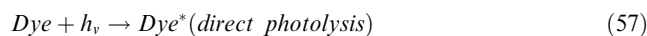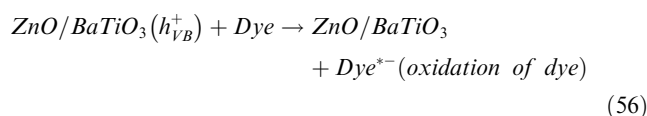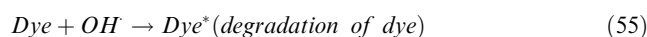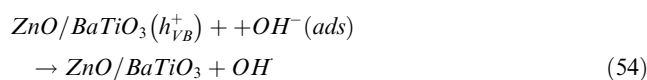
At the photoanode,

$$BiOBr + h_v \rightarrow h^+ + e^- \tag{48}$$

$$RhB + h^+ \rightarrow degradation product \tag{49}$$

At the cathode,

$$O_2 + 4H^+ + 4e^- \rightarrow 2H_2O \tag{50}$$

$$O_2 + 2H^+ + 2e^- \rightarrow H_2O_2 \tag{51}$$

Besides, for the removal of Reactive Red 120 (RR120), Ong et al. (Ong et al., 2019) employed a PFC having as photoanode a $ZnO/BaTiO_3$ loaded carbon plate heterojunction. This study confirmed that Z1B1/C/Z1B1 system has the highest dye

removal efficiency (93.67%) due to sufficient ZnO loading into the Z1B3 system and excellent absorption of UV light. The Langmuir-Hinshelwood kinetics model illustrated a good agreement ($R^2 \approx 1$) between the kinetic model and the experimental data. The Z1B1/C/Z1B1system has the highest rate constant ($0.3554\,h^{-1}$) which shows the higher removal efficiency rate of the RR120 (Ong et al., 2019). However, the direct photolysis is dramatically slower than the other processes and has the lowest rate constant of aerated PFC system. The possible reactions for RR120 degradation are described in the following equations (Ong et al., 2019):

Photoanode

$$ZnO/BaTiO_3 + h_v \rightarrow ZnO/BaTiO_3 \left(e_{CB}^- + h_{VB}^+ \right) \tag{52}$$

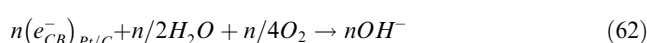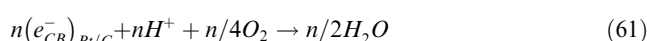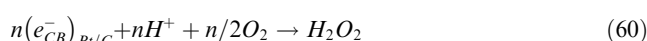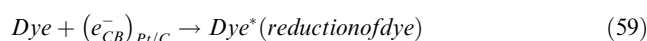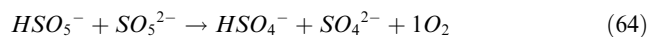$$ZnO/BaTiO_3 \left(h_{VB}^+ \right) + H_2O \rightarrow ZnO/BaTiO_3 + OH^- + H^+ \tag{53}$$

$$ZnO/BaTiO_3 \left(h_{VB}^+ \right) + +OH^- (ads) \\ \rightarrow ZnO/BaTiO_3 + OH \tag{54}$$

$$Dye + OH \rightarrow Dye^* (degradation\ of\ dye) \tag{55}$$

$$ZnO/BaTiO_3 \left(h_{VB}^+ \right) + Dye \rightarrow ZnO/BaTiO_3 \\ + Dye^{*-} (oxidation\ of\ dye) \tag{56}$$

$$Dye + h_v \rightarrow Dye^* (direct\ photolysis) \tag{57}$$
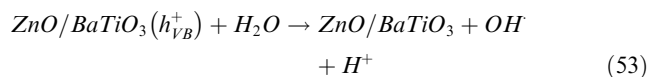
Cathode (in the presence of oxygen)

$$\left(e_{CB}^- \right)_{Pt/C} + O_2 \rightarrow \cdot O_2^- \tag{58}$$

$$Dye + \left(e_{CB}^- \right)_{Pt/C} \rightarrow Dye^* (reduction of dye) \tag{59}$$

$$n \left(e_{CB}^- \right)_{Pt/C} + nH^+ + n/2O_2 \rightarrow H_2O_2 \tag{60}$$

$$n \left(e_{CB}^- \right)_{Pt/C} + nH^+ + n/4O_2 \rightarrow n/2H_2O \tag{61}$$

$$n \left(e_{CB}^- \right)_{Pt/C} + n/2H_2O + n/4O_2 \rightarrow nOH^- \tag{62}$$

Li et al. (2019) (Li et al., 2019) investigated the effects of adding peroxymonosulfate (PMS) into a PFC with TiO_2/Ti photoanode and Pt cathode on TC removal from aqueous solution. The results demonstrated that the addition of PMS could significantly enhance the TC decomposing and accelerate the reaction rate because it has a strong oxidative capacity and can inactivate part of TC. When PMS is activated in presence of UV irradiation (Eqs. (63) and (64)), the produced sulfate radical, $^\bullet OH$, singlet oxygen ($^1O_2$) and PMS direct oxidation can improve the TC degradation (Sharma et al., 2015; Chen et al., 2018; Yang et al., 2018). Furthermore, adding PMS to the PFC can play the role of sacrificial agent that reacts with e^- (Eqs. (65) and (66)) (Sayed et al., 2017) and decreases the recombination of photogenerated e^- and h^+ on the photoanode, thus increasing the production of reactive radicals.

$$HSO_5^- + h_v \rightarrow 2SO_4 \cdot^- + OH \tag{63}$$

$$HSO_5^- + SO_5^{2-} \rightarrow HSO_4^- + SO_4^{2-} + 1O_2 \tag{64}$$

$$HSO_5^- + e^- \rightarrow OH + SO_4^{2-} \qquad (65)$$

$$HSO_5^- + e^- \rightarrow SO_4^{\cdot-} + OH^- \qquad (66)$$

In summary, Table 2 illustrates a summary of the different works tackling the issue of pollutant degradation with various PFCs systems.

Table 2. Degradation of different pollutants in PFCs (Chen et al., 2014; Wu et al., 2015; Tang et al., 2014; Yang et al., 2015; Bai et al., 2016; Chen et al., 2012; Li et al., 2014).

2.1. Bacteria inactivation

Real wastewater contains countless microorganisms and bacteria types that can threaten human health and environmental stability (Zhang et al., 2018). Because conventional disinfection processes e.g. chlorination have led to the generation of toxic byproducts (Ren et al., 2009), there has been a great interest in recent years in the promotion of photocatalysis for disinfection process. The first example of semiconductor photocatalysis used as a disinfection process was reported by Matsunaga et al. (Matsunaga et al., 1985). Since then, due to its safety, low cost and efficiency, the photocatalytic disinfectant TiO_2 has been studied. However, its low quantum efficiency and absorption only near the UV region (400 nm) limit its practical application. So far, many efforts to increase the photocatalytic performance and use of visible light from TiO_2 with rectification methods such as impurity doping, metallization, sensitivity and coating, to extend the edge of TiO_2 adsorption to the optical region can be seen (Yu et al., 2005; Elahifard et al., 2007; Wang et al., 2019; Shanmugam et al., 2020). However, the correction processes are complex and the prepared samples usually suffer from disadvantages e.g. low stability. In recent years, the development of PFCs to inactivate bacteria has become such an important issue that the technology can use a combination of different nanomaterials for use in photocathodes and photododes to significant efficiencies to inactivate bacteria.

Lam et al. (2020) applied a PFC with $TiO_2/ZnO/Zn$ as anode and CuO/Cu as cathode for greywater and bacteria removal and simultaneous energy generation. They found that E. coli cells decreased significantly after 60 min process in PFC. Such efficient treatment efficiency of PFC was due to action of ROS, containing $^\bullet O_2^-$, $^\bullet OH$, H_2O_2, and h^+ by anodic $TiO_2/ZnO/Zn$, which could directly inactivate the bacterial cells.

3. Power generation

3.1. Electricity generation

Under LR, the e^- and h^+ of a semiconductor is separated and a photovoltage is created. The photo-generated h^+ and e^- are the major cause of oxidation and reduction in the n-type and p-type semiconductors, respectively (Zarei et al., 2012; Alikarami et al., 2019). The fuel used to feed a PFC can be either organic or inorganic and it is dissolved in the electrolyte of anode compartment (Ong et al., 2019; Lianos, 2017). The compounds with the CxHyOz structure (alcohols, diols, organic acids, and carbohydrates), usual products of biomass, are the most efficient organic fuels (Sfaelou and Lianos, 2016).

In the system, as a sustainable green technology, it is capable of decomposing organic pollutants and producing electricity simultaneously (Sui et al., 2017) as LR of photocatalytic sites of photoanode in a certain range of wavelengths led to the production of $e^- - h^+$ pairs (Zhao et al., 2017; Zeng et al., 2018; Xia et al., 2016) (Fig. 2). However, in order to ensure that the photogenerated e^- would be excited from the photocatalyst VB to the CB, light energy ($\geq$ than the photocatalyst Eg) is required. The h^+, which have strong oxidability to decompose different organics, react with the organic pollutants to oxidize and degrade them to CO_2, e^- and protons ($C_xH_yO_z + ^\bullet OH \rightarrow CO_2 + H^+ + e^-$) (Lee et al., 2018; Khalik et al., 2017). At this time, , the e^- generated from photocatalysis and oxidation of organics at the photoanode side are transferred to the cathode side, generating electricity (Xie and Ouyang, 2017; Xia et al., 2016).

It is noteworthy that organic fuel oxidation, or an inorganic sacrificial agent (such as S^{-2}, SO_3^{-2},...) or H_2O itself leads to the electricity generation and H_2 production, while electricity alone is generated in the presence of O_2 (Lianos, 2017). Indeed, a PFC can operate in two main operation manners: electricity or H_2. production In the absence of O_2, PFC produces molecular H_2 either by protons reduction (at acidic pH) or by water reduction (at alkaline pH) (Sfaelou and Lianos, 2016). The potential discrepancy between the Fermi levels of two electrodes creates the driving force that causes e^- transfer from photoanode to the cathode. For practical aims, the function of the cell can be approximated using the following strategies. The photoanode potential for n-type semiconductor photocatalysts is close to the CB potential (Lianos, 2017).

For the cell efficiency evolution, the first aspect considered is the estimation of produced e^- number as a percentage of absorbed photons. This is indicated by the incident photon-to-e^- conversion efficiency (IPCE) value. It can be calculated by the Eq. (67) (Lianos, 2011; Varghese and Grimes, 2008):

$$IPCE(\%) = \left[\frac{1240 \times J_{SC}}{\lambda \times P} \right] \times 100 \qquad (67)$$

where Jsc is the short-circuit current density (mA cm^{-2}), P the incident irradiance (mW cm^{-2}), and λ is the incident light wavelength. The number 1240 used in Eq (67) carries the matching units. IPCE% is expected to change between 0 and 100. Sometimes, due to current doubling phenomena, IPCE can have larger values than 100% (Lianos, 2011; Antoniadou et al., 2012).

Another parameter used to express the PFC efficiency is the Fill factor (FF). It is computed using Eq. (68) (O'regan and Grätzel, 1991):

$$FF = P_{max}/J_{SC}V_{SC} \qquad (68)$$

where P_{max} represents the real maximum power density (as obtained from the JV vs. V plot) and $J_{sc}V_{SC}$ is the theoretical maximum power density. The FF also shows the amount of diversion between the actual maximum power density produced and the product of $J_{sc}V_{SC}$. It is mentioned that pure electrolyte with no organic additive shows the smallest J_{sc}, V_{SC}, and P_{max}.

The next parameter employed for all types of fuel cells is power density. The generated power per unit anode area is calculated by Eq. (69) (Lee et al., 2016).

$$P = J \times V \qquad (69)$$

where P is the power density (mW cm^{-2}), J is the current density (mA cm^{-2}), and V is the voltage_(mV).

In the case of PFC performance for the degradation of pollutants, a parameter called degradation efficiency or removal efficiency is applied. It is estimated by the Eq. (70) (Li et al., 2019):

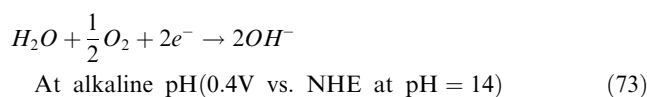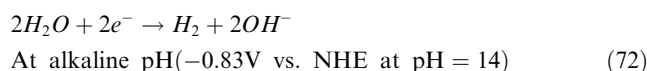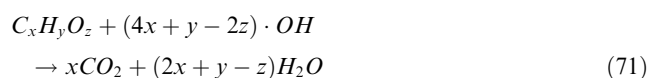$$Degradation(\%) = \frac{C_0 - C_t}{C_0} \times 100 \qquad (70)$$

where C_0 illustrates the initial concentration of pollutant solution and C_t expresses the pollutant concentration at time t.

Many studies focused on improving different aspects of a PFC. For example, a hybrid system of PFC-peroxicoagulation (PFC-PC) was introduced to decompose organic pollutants and to simultaneously produce electricity (Nordin et al., 2019). In this hybrid system, three forms of photocatalysts (TiO$_2$, ZnO, and α-Fe$_2$O$_3$ immobilized on carbon_cloth –CC-) were employed asphotoanodes and degradation of Amaranth dye (93.8%) were obtained (Nordin et al., 2019). Most of the research (Chen et al., 2012; Xia et al., 2016; Liu et al., 2011; Li et al., 2013; Li et al., 2015; Yang et al., 2014) was focused on the operating parameters and optimal performance. The Ho research group reported the effect of different DO concentrations on the mechanism of electricity generation and dye degradation (diazo dye RG19) in the single-chambered PFC based on ZnO/C photoanode (Lee et al., 2018). RG19 has a high resistance to microbial and chemical decomposition (Zuorro and Roberto, 2014). However, the RG19 degradation rate and the electricity generation was raised under high DO concentration (Wang et al., 2019). In all the previous studies, the used systems are single photoelectrode PFC consisting of one photoelectrode (photoanode). It should be noted that systems with dual photoelectrodes of photoanode and photocathode were also proposed (Liu et al., 2016; Bai et al., 2016; Chen et al., 2012; Pan et al., 2018). A dual photoelectrode PFC is formed from an n-type semiconductor photoanode and p-type photocathode. Under light/UV radiation, both photoelectrodes can produce e^-- h^+ pairs. The more negative Fermi level of the photoanode compared to the photocathode forms a bias that led to the e^- migration from the photoanode via the external circuit incorporated into the photocathode h^+ (Wu et al., 2015; Chen et al., 2012). The accumulation of h^+ occurs on the photoanode and of e^- on the photocathode; therefore, it is a Z-scheme (Tada et al., 2006; Maeda, 2013; Zhou et al., 2014).
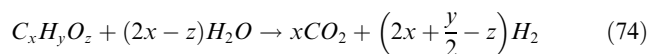
3.2. Hydrogen generation

As we know, solar energy can be turned into useful forms of energy (electricity or chemical energy) using photoelectrochemical cells (PECs). Since the (Fujishima and Kenichi, 1972) paper, the H$_2$ generation through photocatalysis has been the topic of exhaustive studies. In fact, one way to store energy is to convert solar into chemical energy, particularly H$_2$. The photoelectrochemical conversion of solar energy provides the most promising routes for this purpose (Sfaelou and Lianos, 2016; Darbandi et al., 2019). Because of its zero carbon emission, high heat combustion, high energy capacity per unit volume, simple generation and on-site storage, hydrogen is considered a key clean energy option (Veziroğlu, 2008; Ruiz-Gómez, 2013; Kelly and Thomas, 2008). As any standard

PEC, oxidation_half-reaction on the photoanode of PFC is balanced by reduction_half-reaction on the cathode. The reduction_half-reaction does not originally depend on the organic fuel type or inorganic sacrificial agent but it is a standard reaction affected merely by pH and O$_2$ (Sfaelou and Lianos, 2016; Michal et al., 2014; Papagiannis et al., 2020). Therefore, oxidation half-reaction (71) is balanced by either half-reaction (72) or (73) (depending on if there is an inert environment or O$_2$ is present) (Lianos, 2017) (Fig. 2).

$$C_xH_yO_z + (4x + y - 2z) \cdot OH$$
$$\rightarrow xCO_2 + (2x + y - z)H_2O \qquad (71)$$

$$2H_2O + 2e^- \rightarrow H_2 + 2OH^-$$
At alkaline pH(−0.83V vs. NHE at pH = 14) (72)

$$H_2O + \frac{1}{2}O_2 + 2e^- \rightarrow 2OH^-$$
At alkaline pH(0.4V vs. NHE at pH = 14) (73)

The overall reaction becomes Eq. (74) (Lianos, 2017); which is consistent with photo electrocatalytic reforming for hydrogen production (Chiarello et al., 2010; Nomikos et al., 2014).

$$C_xH_yO_z + (2x - z)H_2O \rightarrow xCO_2 + \left(2x + \frac{y}{2} - z\right)H_2 \qquad (74)$$

For hydrogen generation, the efficiency of solar to H$_2$ (η_{STH}) is determined as (Li et al., 2013; Kim et al., 2016):

$$\eta_{SHT} = \frac{J(mA.cm^{-2}) \times (1.23 - V_{app})(V)}{P(mW.cm^{-2})} \times 100 \qquad (75)$$

where $V_{app} = V_{bias}$ -V_{oc}. V_{oc} is the open circuit potential assessed under the same conditions as the bias potential (Khan et al., 2002; Lin et al., 2015).

In reality, η_{STH} represents the device efficiency and indicates its current generation capacity. However, the H$_2$ generation is not guaranteed by the flow of current and the η_{STH} determination should be accompanied by *faradaic efficiency* calculation (the percentage of current converted into H$_2$) (Lianos, 2017):

$$1\frac{\mu mol}{min} \rightarrow \frac{10^{-6} \times 6.022 \times 10^{23} \times 2 \times 1.6 \times 10^{-19}C}{60S} = 3.21mA \qquad (76)$$

Furthermore, as discussed in Section 3.1, a new application of PFC was introduced for H$_2$ generation by a solar-driven dual-photoelectrode PFC (Wu et al., 2015). To design such a system, with the aim of simultaneously generating electricity and hydrogen, the photoanode should be an n-type semiconductor and have a good photocatalytic activity (Wu et al., 2015). The photocathode should be a p-type semiconductor whose E$_{cb}$ (*vs.* NHE) should be more negative than 0 V ($E^\circ_{H^+/H_2}$) for the purpose of hydrogen generation, such as Cu$_2$O (Wang et al., 2013; Huang et al., 2011).

4. Photoanodes

4.1. The effects of different photoanode materials

Considering that the photoanode plays a significant role, the researchers try to reduce the photoanode limitations by

Y. Vasseghian et al.

Table 2 Degradation of different pollutants in PFCs.

Authors/Year	Photoanodes	Photocathodes	Substrates	Degradation Efficiency (%)		Process Time (min)	Maximum power density (P_{max}, W m^{-2})	Open circuit voltage (V_{oc}, V)	Refs.
Chen et al./2012	WO$_3$/W	Cu$_2$O/Cu	Rhodamine B Congo Red Phenol	63 74 58		300	0.677	0.33	(Chen et al., 2012)
Chen et al./2014	nanopore WO$_3$/W	Pt/PVC	Methylene Blue	91		90	1.33	0.38	(Chen et al., 2014)
Tang et al./2014	TiO$_2$/Ti disk	Pt black/Pt electrode	Rhodamine B Reactive Brilliant Red X-3B	≈ 100 ≈ 100		240	5.049 6.788	0.953 0.978	(Tang et al., 2014)
Li et al./2014	TiO$_2$/FTO	carbon paper deposited with carbon black and Pt black	Methylene Blue	83.9		360	5.80	1.06	(Li et al., 2014)
Wu et al./2015	TiO$_2$ NRs/FTO	C/Cu$_2$O NWAs/Cu mesh	Phenol	84.2 of TOC		480	7.3	0.41	(Wu et al., 2015)
Yang et al./2015	TiO$_2$ nanotube array/Ti rotating-disk	Cu rotating-disk		Anode Chamber	Cathode Chamber	120	-	(Yang et al., 2015)	(Wu et al., 2015)
			Rhodamine B	96.8	89.8				
			Reactive Brilliant Red X-3B	69.8	50.9				
			Methylene Blue	92.9	84.7				
			Glucose	86.9	54.8				
			Rhodamine B/ Bisphenol A	93.2	71.3				
Bai et al./2016	BiVO$_4$/TiO$_2$ nano-tubes/FTO	ZnO/CuO nanowires/FTO	Methyl Orange Congo Red Methylene Blue	76 83 90		80	1.16	0.53	(Bai et al., 2016)
Khalik et al./2016	ZnO onto carbon felt	Pt-coated carbon paper	Reactive Black 5	≈ 100		1440	3.35 (Na$_2$SO$_4$ electrolyte), 2.56 (MgSO$_4$ electrolyte) and 2.45 (NaCl electrolyte)	1.129 (Na$_2$SO$_4$ electrolyte), 1.070 (MgSO$_4$ electrolyte) and 1.100 (NaCl electrolyte)	(Khalik et al., 2016)
Lee et al./2016	ZnO/Zn	platinum loaded carbon	Reactive Green 19	100		480	12.696 (Na$_2$SO$_4$ electrolyte), 1.077 (MgSO$_4$ electrolyte) and 2.817 (NaCl electrolyte)	1.128 (Na$_2$SO$_4$ electrolyte), 0.990 (MgSO$_4$ electrolyte) and 1.049 (NaCl electrolyte)	(Lee et al., 2016)
Khalik et al./	ZnO/carbon felt	Pt-loaded carbon	Reactive Black 5	80		360	6.571 (UV) and 16.651 (solar)	0.75 (UV) and 0.82 (solar)	(Khalik et al.,

Table 2 (*continued*)

Authors/ Year	Photoanodes	Photocathodes	Substrates	Degradation Efficiency (%)	Process Time (min)	Maximum power density (P_{max}, W m^{-2})	Open circuit voltage (V_{oc}, V)	Refs.
2017								2017)
Sui et al./ 2017	TiO$_2$/Ti mesh	activated carbon/ poly tetra fluoro ethylene	Rhodamine B	98.5	150	0.222	-	(Sui et al., 2017)
Sui et al./ 2017	TiO$_2$ Ag/ TiO$_2$	biocathode with carbon fiber brushes	Rhodamine B	97.3 99.5	120	0.211 0.318	0.350 0.458	(Sui et al., 2017)
Zhao et al./ 2017	TiO$_2$ TNA	Pt/SiPVC	Methyl Orange	91.98	90	0.84 (PFC) and 1.57 (PFC(Fe^{2+})	0.75 (PFC) and 0.76 (PFC(Fe^{2+})	(Zhao et al., 2017)
			Methylene Blue	98.57		0.65 (PFC) and 1.01 (PFC(Fe^{2+})	0.82 (PFC) and 0.81 (PFC(Fe^{2+})	
			Congo Red	92.36		0.52 (PFC) and 1.24 (PFC(Fe^{2+})	0.84 (PFC) and 0.85 (PFC(Fe^{2+})	
			Tetracycline	68.09		0.48 (PFC) and 0.97 (PFC(Fe^{2+})	0.77 (PFC) and 0.81 (PFC(Fe^{2+})	
Zhao et al./ 2017	TiO$_2$ TNA	Pt-black/Pt	Methyl Orange	97.34	60	3.30 (PFC) and 5.70 (Fenton-PFC)	1.26 (PFC) and 1.23 (Fenton-PFC)	(Zhao et al., 2017)
			Methylene Blue	95.36		2.70 (PFC) and 3.70 (Fenton-PFC)	1.26 (PFC) and 1.26 (Fenton-PFC)	
			Congo Red	93.23		3.00 (PFC) and 4.30 (Fenton-PFC)	1.25 (PFC) and 1.25 (Fenton-PFC)	
			Tetracycline	73.80		2.50 (PFC) and 3.40 (Fenton-PFC)	1.20 (PFC) and 1.21 (Fenton-PFC)	
Lee et al./ 2018	ZnO loaded carbon	platinum loaded carbon	Reactive Green 19	37	480	0.0028	-	(Lee et al., 2018)
Lee et al./ 2018	immobilizing ZnO onto zinc	platinum loaded carbon	Reactive Green 19	93-sunlight 86-ultraviolet	480	0.026 (sunlight) and 0.021 (ultraviolet)	0.704 (sunlight) and 0.814 (ultraviolet)	(Lee et al., 2018)
			Acid Orange 7	62-sunlight 74-ultraviolet		0.010 (sunlight) and 0.012 (ultraviolet)	0.669 (sunlight) and 0.683 (ultraviolet)	
			Methylene Blue	87-sunlight 36-ultraviolet		0.032 (sunlight) and 0.017 (ultraviolet)	0.924 (sunlight) and 0.855 (ultraviolet)	
Nahyoon et al./ 2018	Fe/GTiP	ZnIn$_2$S$_4$	Rhodamine B	79.5	100	–	0.4	(Nahyoon et al., 2018)
Li et al./ 2018	TiO$_2$ TNA on the titanium sheet	platinum plate	Methyl Orange	92	240	0.110 (PFC) and 0.1925 (PFC/PS)	0.682 (PFC) and 0.856 (PFC/PS)	(Li et al., 2018)
Kee et al./ 2018	ZnO/Zn	CuO/Cu	Methyl Green	92	240	0.164 (Na$_2$SO$_4$ electrolyte), 0.142 (MgSO$_4$ electrolyte), 0.159 (NaCl electrolyte) and 0.054 (No electrolyte)	0.919 (Na$_2$SO$_4$ electrolyte), 0.798 (MgSO$_4$ electrolyte), 0.898 (NaCl electrolyte) and 0.702 (No electrolyte)	(Kee et al., 2018)
Lu et al./ 2018	BiOBr/TiO$_2$ TNAs with 15 SILAR	Pt	Rhodamine B	99.7	240	0.022	0.498	(Lu et al., 2018)
Zeng	TiO$_2$/WO$_3$/W	Pt/BJS	Rhodamine B	99.3	180	0.694	0.792	(Zeng

(*continued on next page*)

Table 2 (*continued*)

| Authors/Year	Photoanodes	Photocathodes	Substrates	Degradation Efficiency (%)	Process Time (min)	Maximum power density (P_{max}, W m^{-2})	Open circuit voltage (V_{oc}, V)	Refs.
et al./2018			Methylene Blue	98.6		0.588	0.768	et al., 2018)
			Phenol	91.7		0.498	0.753	
			Bisphenol A	95.2		0.526	0.766	
			Dichlorophen	96.5		0.563	0.757	
			Tetracycline	92.3		0.554	0.772	
Deng et al./2018	Ag-TiO$_2$	Pt	4-chlorophenol	32.6	360	0.03398	0.492	(Deng et al., 2018)
			Phenol	37.9		0.08995	0.499	
			Tetracycline	96.4		0.10212	0.499	
Ong et al./2019	ZnO/BaTiO$_3$loaded carbon plate heterojunction	Z1B1/C/Z1B1	Reactive Red 120	93.67	480	0.005284	0.35	(Ong et al., 2019)
Rabé et al./2019	Z-scheme g-C$_3$N$_4$/Fe^0/TiO$_2$	WO$_3$	berberine chloride	91	90	16.4	0.8	(Rabé et al., 2019)
Li et al./2019	TiO$_2$/Ti	platinum	Tetracycline	90.14	60	0.015 (PFC) and 0.034 (PFC/PMS)	0.587 (PFC) and 0.749 (PFC/PMS)	(Li et al., 2019)
Wang et al./2020	TiO$_2$ nanorods	Cu$_2$O	Formaldehyde	–	3.3	–	0.58	(Wang et al., 2020)
Yu et al./2020	Ag$_3$PO$_4$ g-C$_3$N$_4$ Ag$_3$PO$_4$@g-C$_3$N$_4$	Cu$_2$O	Tetracycline	30 20.82 76	240	0.0416 0.00067 0.0606	0.095 0.080 0.18	(Yu et al., 2020)
Lam et al./2020	TiO$_2$/ZnO/Zn	CuO/Cu	Escherichia coli	99	60	0.172	0.868	(Lam et al., 2020)
Chen et al./2020	TiO$_2$ nanotube arrays	Pt	Ofloxacin	96.8	60	0.247	1.35	(Chen et al., 2020)
Lam et al./2020	ZnO/Zn	Pt	Sunset yellow	–	240	0.000565	0.411	(Lam et al., 2020)
			Phenol	–		0.00031	0.398	
	WO$_3$/ZnO/Zn		Sunset yellow	84.6		0.001052	0.823	
			Phenol	67.5		0.000574	0.759	
Kee et al./2020	TiO$_2$/ZnO/Zn	TiO$_2$/CuO/Cu	Palm oil mill effluent treatment	90	240	0.734	1.173	(Kee et al., 2020)
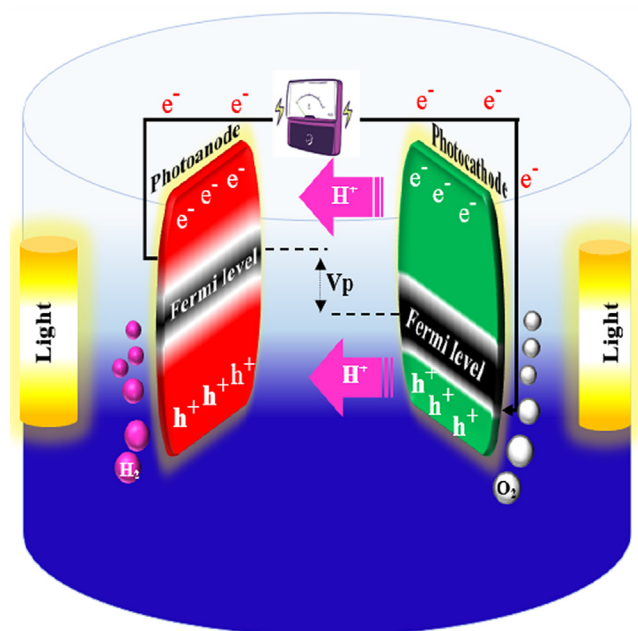
Fig. 2 Electricity generation and hydrogen production in PFC.

improving the photocurrent and VLR response and decreasing the cost of construction and practical applications (Venkatkarthick et al., 2017; Venkatkarthick et al., 2016). Moreover, the fast induced e^- and recombination of e^--h^+ pairs in the_photoanode would limit the photoelectrochemical_reaction (Khataee et al., 2011), the Eg and the recombination of photogenerated $e^-$and h^+ are two main parameters that affect the photocatalytic activity to produce $^\bullet OH$ and electricity (Ong et al., 2018) (Fig. 3).

Accordingly, the photoanode_material with different Eg, recombination rate and features of e^- mobility play a fundamental role in the PFC systems, which can affect their performance. For these, numerous photoanode such as TiO_2, ZnO, WO_3, α-Fe_2O_3, $BiVO_4$, $BaTiO_3$ have been studied so far (Ong et al., 2019; Strataki et al., 2010; Monfort et al., 2016; Gan et al., 2014; Horiuchi et al., 2013; Bhatt and Lee, 2015; Pop et al., 2015; Gao et al., 2014; Alexander et al., 2008). Based on a recent review (Lianos, 2017), most studies on the_PFC to date are focused on TiO_2_photoanode. Usually, the Degussa P25 TiO_2 powder (UV activated) is the commercially accessible photocatalyst used for the PFC photoanode (Kaneko et al., 2006; Seger et al., 2012; Antoniadou and Lianos, 2010). TiO_2 has raised an excessive interest as photocatalyst among semiconductors and, since it possesses stable physical and chemical features such as low cost, easy to prepare, nontoxicity, outstanding stability, and excellent electronic and optical properties (Li et al., 2014; Liu et al., 2011). For instance, Kaneko et al. (Kaneko et al., 2006) used a nanoporous titanium dioxide film_photoanode and an O_2-reducing cathode to construct a PFC. Then, Lianos et al. (Lianos, 2011), Liu et al. (Liu et al., 2012; Liu et al., 2011) and Li et al. (Li et al., 2013) obtained efficient electricity production and simultaneous refractory organic compounds degradation using different types of TiO_2 photoanodes such as TiO_2 nanoparticles and TiO_2 nanotube arrays/Ti. Due to its higher Eg (3.0–3.2 eV), TiO_2 can only absorb 4% solar LR (Wang et al., 2014). Hence, the use of TiO_2 is more suitable

under UV compared to the solar counterpart (Hashimoto et al., 2005) and, under UV irradiation, the photogenerated e^- can only migrate from TiO_2 to the cathode (Paulose et al., 2007). This limits the potential of PFC in industrial applications with solar energy. The photogenerated e^- and h^+ are easy to recombine in TiO_2 which reduces photocatalytic_degradation (Li et al., 2019).

The literature presents many viewpoints concerning the efficiency raise of organic wastewater treatment by decreasing the adverse effects of e^--h^+ recombination and improving the VLR absorption ability. This includes metal doping (Kim et al., 2015; Li et al., 2013), coupling other semiconductors with TiO_2 (Jiao et al., 2014) and changing the fabrication methods to optimize the micro/nanostructure of TiO_2 (Pang et al., 2014). Because the functional characterization of materials greatly depends on their micro/nanostructure, TiO_2 has been deposited as different types of nanostructures including nanoparticles, nanorods, nanotubes, nanowires, etc., (Sfaelou and Lianos, 2016) and different deposition methods were used for photoanode fabrication using powdered TiO_2 (spin coating (Kaneko et al., 2005), screen printing (Panagiotopoulou et al., 2010), and doctor blade method (Antoniadou et al., 2010).

Other than TiO_2, the most popular metal oxide semiconductors which have been used by researchers as photocatalyst in the photoanode so far are ZnO, WO_3, $BiVO_4$, α-Fe_2O_3 and recently $BaTiO_3$ (Ong et al., 2019; Sfaelou and Lianos, 2016). Based on the recent review by Sfaelou and Lianos (Sfaelou and Lianos, 2016), they are not better than TiO_2, if all parameters are considered together. The only reason for selecting some other metal oxide semiconductors is to use a material that absorbs VLR and does not necessitate the presence of a sensitizer, especially, the toxic metal sulfides (CdS) and selenides (ZnSe).

Hematite (α-Fe_2O_3) is one of the semiconductors employed as a photocatalyst in the PFC photoanode. α-Fe_2O_3 is a low-cost n-type semiconductor with relatively small Eg (2.0–2.2 eV) able to absorb the close -infrared spectrum (up to 600 nm) and roughly 40% of the solar energy. Nonetheless, the photocatalytic activity of α-Fe_2O_3 is affected by some parameters include short diffusion lengths of h^+ (2.0–4.0 nm), high carrier recombination, confined charge transport feature and electrical conductivity (Nordin et al., 2019).

In the photocatalysis field, ferroelectric materials are a novel alternative to classic materials. Due to its robust ferroelectric feature, $BaTiO_3$ with perovskite structure has attained much interest (Cao et al., 2014). $BaTiO_3$ with a wide Eg (3.18 eV) has been considered to remove different types of dyes such as methyl orange (Liu et al., 2012) and Rhodamine B (Cui et al., 2013).

4.2. Photoanode materials characterization

The characterization of photocatalyst used in the photoanode compartment is a key step in the construction and evaluation of PFC systems. This involves structural, optical, and photoelectrochemical characterizations. The photoanodes morphology is identified by using the scanning electron microscopy (SEM) technique. In fact, this technique can provide sufficient information about the electrode morphology by providing low/high magnification and cross-sectional images. The result of SEM images showed the well-aligned tube-like morphology

of the TiO$_2$ electrode fabricated by electrochemical anodization method with an average diameter of 0.5 μm and length of 5 μm. SEM images indicate the naturally created Schottky-type contact between the TiO$_2$ nanotubes and Ti substrate, which can prepare a unidirectional electric channel for the transfer of photogenerated e^-. Due to their geometric characteristics, these nanotubes can absorb reflected/refracted light, thus minimizing the photon's loss resulting from light scattering in the liquid. In other words, the multi-tube structure of TiO$_2$ nanotube arrays can increase the semiconductor surface area, improving the absorption properties and LR utilization, and also adsorption of organic pollutants at the electrode surface (Li et al., 2018; Sui et al., 2015).

Detailed microstructural features of the photoanodes are studied by transmission electron microscopy (TEM) and high-resolution transmission electron microscopy (HR-TEM). For example, the presence of Ag nanoparticles (Sui et al., 2017) and CdS-ZnS sensitizers (He et al., 2018) on the TiO$_2$ nanotubes was further confirmed by TEM and HRTEM, which revealed the well-defined lattice fringes of the Ag (Zhao et al., 2017) plane in Ag/TiO$_2$ (Sui et al., 2017).

The crystalline structures of the photocatalysts are analyzed by X-ray diffraction (XRD) (Sfaelou and Lianos, 2016). Hence, during the fabrication of TiO$_2$-based photocatalysts used in PFCs as photoanode, the XRD can be applied as a powerful technique to confirm the successful formation of the photo-catalytically active type (He et al., 2018). The identifying peaks in the XRD patterns represent that TiO$_2$ was easily crystallized in anatase and rutile phases. Stronger diffraction peaks are observed for the anatase phase compared to the rutile counterpart, suggesting the content of the anatase phase is higher. It is evident that the peaks intensity of TiO$_2$ is much stronger after calcination treatment.

As noted, the photoelectrochemical efficiency of photoanode can be characterized by the cyclic voltammetry (CV), linear sweep voltammetry (LSV) and electrochemical impedance spectroscopy (EIS) measurements (He et al., 2018). There is a clear difference between them when the applied voltage $vs.$ the Ag/AgCl reference electrode is more than -0.5 V; the current density can reach 2.42 mA cm^{-2} (under LR) and 0 (without LR). This result illustrated that the developed photoanode has an excellent activity under VLR.

The Ag/TiO$_2$ and TiO$_2$ LSV curves show that, in the absence of LR, the photocurrent value swiftly decreases to zero. At 0.4 V electrode potential, the Ag/TiO$_2$ photocurrent (3.9 mA) is much higher than that of TiO$_2$ (1.9 mA). This indicates the lower recombination rate of photo-induced e^-- h^+ pairs, as well as the higher LR absorbance for the electrode, which can improve the bio-PFC performance.

UV–Vis diffuse reflectance spectroscopy (UV–Vis DRS) as an optical characterization method commonly used in order to investigate the ability of prepared photoanodes to respond to the VLR. Eg is an important feature of the semiconductors which can be computed with the following formula (Bai et al., 2016):

$$\alpha h\upsilon = A\left(h\upsilon - E_g\right)^n \tag{77}$$

where α is the absorption coefficient, $h\upsilon$ is the photon energy, A is a constant and n indicates the type of optical transition of semiconductor (n = 1 for a direct transition and n = 4 for an indirect transition) (Jun et al., 2012). As previously reported,

for photocatalysts such as TiO$_2$, ZnO, BiVO$_4$, which are indirect Eg semiconductors (Bai et al., 2016), n is equal to 4.

In the UV region, pure TiO$_2$NTs has 361 nm absorption edge. In the visible region, BiVO$_4$/TiO$_2$NTs (as a composite photocatalyst) have a 530 nm absorption edge and is about 170 nm red-shifted (compared to pure TiO$_2$NTs). This indicates that TiO$_2$NTs can extend the BiVO$_4$ absorption spectrum into the visible region. The Eg of pure TiO$_2$NTs and BiVO$_4$/TiO$_2$NTs was estimated to be 3.32 and 2.34 eV. This result reveals that the incorporation of BiVO$_4$ into TiO$_2$NTs would lead to a lower Eg.

In other studies, the UV–Vis showed that the combination TiO$_2$ semiconductor with nanoparticles such as Ag (Sui et al., 2017) and quantum dots such as CdS and CdS-ZnS (He et al., 2018; Wang et al., 2014) leads to absorption band shifting to the visible region. Consequently, the response of prepared photoanodes to VLR is an improved, and effective way to harvest solar radiation being achieved.

The photoluminescence (PL)_spectrum analysis is also employed to evaluate the separation and recombination efficiency of photoinduced e^- and h^+. For example, the Ag/TiO$_2$ and TiO$_2$ electrodes illustrated analogous broad PL emission bands (Sui et al., 2017). The PL spectrum of Ag/TiO$_2$ shows a weak peak compared to TiO$_2$, implying that the Ag doping on TiO$_2$ nanotubes increases the probability of e^--h^+ recombination that leads to PL_intensity reduction.

5. Photocathodes

5.1. Photocathode materials for electricity generation and dye degradation

Due to the presence of over potential developed between the cathode and electrolyte, reduction reactions do not occur automatically. To overcome this overpotential, an electrocatalyst is necessary. Since the role of the electrocatalyst is to create a large interface between two phases, facilitate the e^- exchange with electrolyte, and eliminate the over-potential, the counter electrode operation potential is similar to the electrochemical potential of the corresponding reduction reactions (Sfaelou and Lianos, 2016) (Fig. 3). A standard and common electrocatalyst used for PFC cathodes fabrication is a mixture of carbon black with nanoparticulate Pt (Pt/C) (Antoniadou and Lianos, 2010). An example of using Pt-coated carbon for O$_2$ reduction reaction at the surface of the cathode is (Kaneko et al., 2009). The reaction at Pt-coated carbon is dependent on O$_2$ accessibility. In the presence of O$_2$, the reaction produces water, while the hydrogen evolution reduction occurs in the absence of oxygen (Wang et al., 2014). The use of an O$_2$-reducing cathode involves a continuous entry of O$_2$ into the electrolyte. Several constraints such as high cost and low availability of Pt have become major concerns for large scale application of Pt. Furthermore, Pt has the tendency to aggregate so that its efficiency is progressively diminished. Therefore, low-cost materials with comparable activity (that can efficiently substitute Pt) are being developed for PFC applications (Sfaelou and Lianos, 2016). To overcome the aforementioned limitations, the use of different Fermi levels photoanodes and photocathodes is encouraged.

One of the most popular p-type photocatalysts is Cu$_2$O (2.0 eV Eg) (Paracchino et al., 2011). Its CB is well suited for
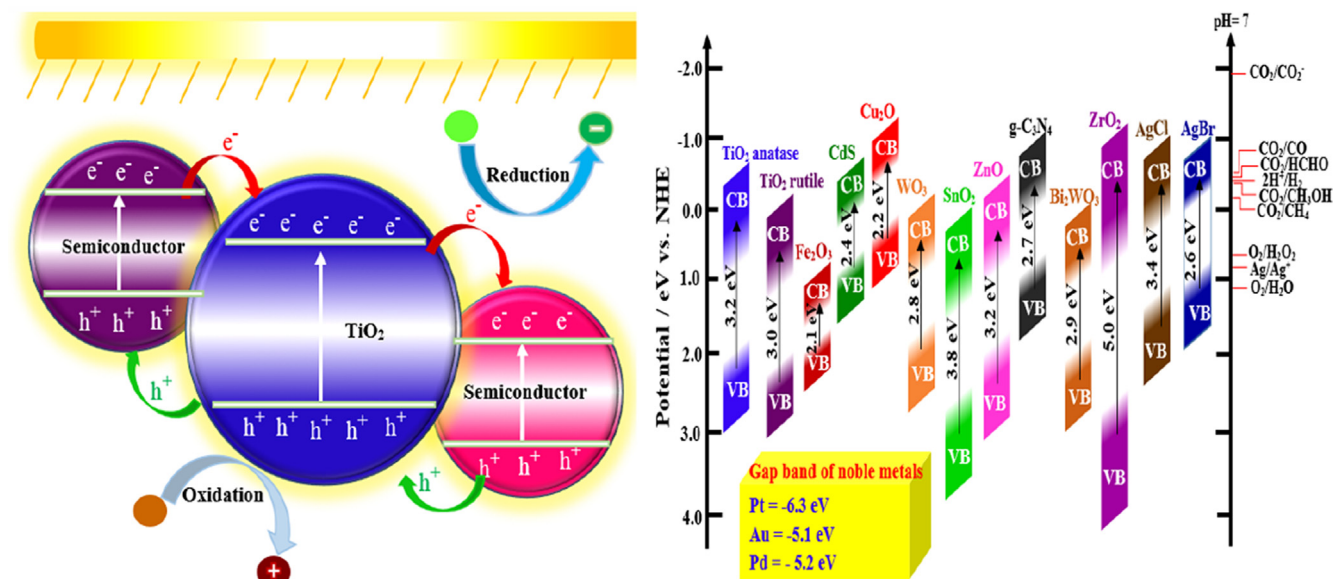
Fig. 3 Reduction/oxidation mechanism in photocatalytic reactions and gap band of some semiconductors which used in photoanode and photocathode of PFC.

water reduction, but for water oxidation, a proper bias is needed. Due to its optimal Eg, Cu_2O can be also activated under VLR, and it was shown that it can be an effective photocathode (Chen et al., 2012). Therefore, in order to construct low-cost PFC systems, Cu_2O can be used to replace Pt. On the other hand, CuO (1.4 eV direct Eg) is another p-type semiconductor abundant in nature that has been proven as stable and effective photocathode (Masudy-Panah et al., 2017; Masudy-Panah et al., 2016).

5.2. Photocathode materials characterization

Various structures and compositions can possess considerably different properties and can, therefore, through complex structure–property relationships, they can affect the overall photoelectrode performance (Esposito et al., 2015). In this respect, the characterization of photocathode materials in the PFC systems is as important as the photoanode counterparts. In general, the techniques used to characterize the photocathodes are the same as those used for the photoanodes characterization (and mentioned in Section 5.1). For example, in order to study the crystalline phase of heterojunction ZnO/CuO NWs photocathode, Bai et al. (Bai et al., 2016) employed XRD analysis. Except for the SnO_2 background which belongs to the FTO_glass, the chief components of photocathode were identified as CuO and ZnO according to the_peak_intensity. Meantime, the CuO reduction leads to small quantities of Cu_2O. It is worth noting that no peaks_of_Cu are observed, suggesting that Cu film was completely transformed into copper oxides (CuO and Cu_2O).

6. Anodic nanocomposites

As previously mentioned, the wastewater organic compounds are an important source of energy. According to the statistics, due to biowaste discharge, about one-third_of_the the global_yearly_energy demand (130 EJ per year) resulting from

organic matter is lost. Therefore, attempts to reach a sustainable methodology that recovers the energy_from this energy-rich_organic_waste and decompose them to non-dangerous products are strongly advisable (Liu et al., 2011). For this purpose, most PFC studies focus_on_developing_TiO_2 photoanode (which can merely respond to UV). To improve the light utilization efficiency and the possibility to use in industrial applications, the development of VLR responsive photoanodes is crucial (Lu et al., 2018). Many PFC works attempted to design the photoanodes by coupling_it_with_narrow Eg semiconductors (that can simultaneously enhance effectiveness and electricity generation). For this reason, many photoanodes (such as CdS-ZnS/TiO_2, $BiVO_4$/TiO_2-NTs, $BiVO_4$/WO_3/W, α-Fe_2O_3/TiO_2/Ti, $ZnFe_2O_4$/TiO_2-NTs, Ag/AgCl/TiO_2, CdS/TiO_2 and BiOBr/Ti) have been investigated (Ong et al., 2019; Li et al., 2019; Zhao et al., 2017). In addition, in expanding the LR absorption from UV_to_visible_region, different doping strategies using metal ions, non-metal ions and different semiconductors with GO have been tested (Mecha et al., 2017). Modifying the_photocatalytic_activity of pure_semiconductor catalyst using metal-ion doping leads the absorption of visible range and causes an increase in the photoreactions. It was shown that GO-based nanocomposites such as Gr–TiO_2 (Liu et al., 2010), Gr–ZnO (Neelgund et al., 2014), Gr–CdS (Thakur et al., 2017), and Gr–SnO_2 (Chen et al., 2017) increase the photocatalytic degradation efficiency (Fig. 4).

An example of using a composite photoanode in the PFC systems is the work of Liu et al (Liu et al., 2011). A short TiO_2_nanotube_array (STNA)-based PFC system was constructed for electrical power generation from different refractory organic compounds and simultaneous wastewater treatment. The current-voltage_characteristics_of PFC systems using different photoanode materials (pure and composite) were compared under solar LR. It was shown that decorating the pure_STNA_electrode_material with narrow Eg semiconductors (e.g. Cu_2O and CdS), under simulated solar LR, significantly increases J_{sc} and JV_{max} values. For the CdS/STNA photoanode, J_{sc} and JV_{max} were 1.66–1.75 and_1.38–2.

41_times_higher than those of the respective pure STNA_pho-toanode for three different organic compounds solution. That means the PFC system can work outdoors_under_solar_irra diation and light a LED indicative lamp by using this composite photoanode material.

7. Photocatalytic fuel cell and Fenton process

As already mentioned, due to its significant advantages, PFC is an important technology for wastewater treatment and simultaneous power generation. Recently, much attention has been paid to the_development_of photoanode and photocathode to improve performance (Li et al., 2014; Bai et al., 2016; Chen et al., 2012; Zang et al., 2014; Wang et al., 2015). During this time, novel photoelectrodes were designed to increase LT absorption and the separation of the e^- - h^+ or surface area, which partially enhances the performance in the degradation of organic pollutants and simultaneous power generation. However, the efficiency is now restricted, as there are many challenges from the aspect of intrinsic semiconductor constraints. The most important constraints of PFCs are the radical reactions taking place on the photoanode and photocathode surfaces. However, the surface area cannot be significantly enlarged, which is a serious constraint on PFCs in the degradation of organic pollutants (Zhao et al., 2017). So how to increase the efficiency of radical reactions that only affects the surface of electrodes is the key to solving this problem. Lately, the Bio electro-Fenton system, which includes MFCs and the Fenton process, has_been_studied as a promising method for organic pollutant treatment (Zhang et al., 2015; Zhuang et al., 2010; Fu et al., 2010; Thor et al., 2020). This integration is an attempt to extend H_2O_2 production technologies that are cost-effective, efficient_and_sustainable for pollutant treatment (Zhang et al., 2015). The e^- produced by a microbial reaction are applied by electro-Fenton reactions to treat pollutants in the MFC cathode. The reaction of ferrous ions with H_2O_2 produced by the process of oxygen reduction leads to $^\bullet OH$ production (Feng et al., 2010). This process is identified as the_electro-Fenton_process (Brillas et al., 2009).

The PFC_system can generate its external voltage through the self-bias between photoanode_and_cathode, the process which is accompanied by degradation of organic pollutants. If ferrous ions are added, a self-bias Fenton-PFC system will be created to decompose organic pollutants and simultaneously produce power. Since PFC is more useful than other fuel cells for the oxidation process of organic_and_inorganic materials, it could be a more appropriate partner for the Fenton process, given the considerable challenges in developing and exploiting these systems. The system can minimize maintenance costs and since it uses a PEC system that employs photoexcitation to generate e^- and h^+ using n-type semiconductor as a photocatalyst, it does not require monitoring (Yang et al., 2014). The hybrid Fenton-PFC_system_has the following characteristics (Zhao et al., 2017):

i. It develops radical reactions from the_electrode_surface to the overall solution with the entry of the Fenton_reac tion_in_the_system, which significantly increases the efficiency of radical reactions in the organic matter degradation and the electrical power generation relative to the traditional PFC.
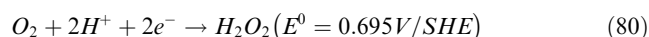
ii. It does not require external H_2O_2 as an oxidizing agent because $HO\cdot$, $HO_2\cdot$, and H_2O_2 can be generated on the electrodes under LR, which decreases operating costs.

iii. It does not need external voltages and additional ferrous_ions_because the self-bias voltage yielded can transmit e^- to the cathode and achieve conversion to Fe^{2+}/Fe^{3+}.

iv. It extremely produces sludge because of the radical reaction by using low levels of ferrous ions.

The mechanism of pollutant removal in the hybrid Fenton-PFC_system is as follows (Nordin et al., 2017):
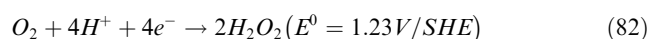
At PFC anode

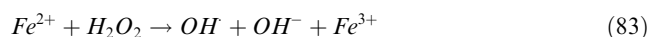$$anode \rightarrow anode(h^+ + e^-) \tag{78}$$

$$h^+ + Reactant \rightarrow Oxidized product \tag{79}$$

At Fenton cathode

$$O_2 + 2H^+ + 2e^- \rightarrow H_2O_2 (E^0 = 0.695 V/SHE) \tag{80}$$

At Fenton anode

$$Fe \rightarrow Fe^{2+} + 2e^- \tag{81}$$

At PFC cathode

$$O_2 + 4H^+ + 4e^- \rightarrow 2H_2O_2 (E^0 = 1.23 V/SHE) \tag{82}$$

Overall Fenton process

$$Fe^{2+} + H_2O_2 \rightarrow OH + OH^- + Fe^{3+} \tag{83}$$

It can be concluded that the hybrid Fenton-PFC system is a promising technology for organic pollutants removal and generating electricity simultaneously. In this hybrid system, PFC is employed to produce e^- to produce H_2O_2 electrons as Fenton's reagent. Fig. 5 illustrates the schematic of the hybrid Fenton-PFC system for pollutant removal. Generally, the unique features of the hybrid Fenton-PFC system result in a fast and stable catalytic system with excellent efficiency (Nordin et al., 2017).

8. Conclusions and recommendations

In this work, a review of the most representative research specific to PFCs for wastewater treatment and synchronous power generation has been performed. Since the performance of PFC is usually specified by the electrodes, most researches focus on the production of electrode materials in recent studies. Given that the features of functional electrode materials are significantly dependent on their structure, recent advances in nanotechnology produces efficient electrodes. In this regard, various nanomaterials were tested such as $CdS–TiO_2$, $CdS/ZnS/TiO_2$, $Ag/AgCl/GO$, $Ag-TiO_2$, WO_3/FTO, $ZnO/BaTiO_3$, ZnO/Zn. These electrodes are based on nanomaterials can led to enhance efficiency of the degradation of organic contaminants, energy performance, or both. But among these nanomaterials, TiO_2 is employed as the most efficient photodanode catalyst, due to its high oxidizing power, excellent stability low cost, low recombination rate (that can enhance efficiency in the utilization of the photogenerated e^- to produce the Fenton's reagent) and also because it is an n-type semiconductor. But, this application is still limited because TiO_2 only responds to UV light, which makes up

< 5% of solar energy, and the recombinant high electron / hole pair reduces a large amount of energy lost due to heat, decreasing quantum efficiency and thus treatment performance. Thus, the use of effective methods to overcome TiO_2 deficiency is essential to enhance the catalytic activity of the anode. Among the researches, TiO_2 modification with a narrow band gap semiconductor shows excellent potential. Because such modifications can effectively enlarge the catalyst light response area due to the semiconductor excitation of the narrow band gap, especially in the visible light region. On the other hand, the heterogeneous performance between the two semiconductors separates the generated carriers from the photogenerated and
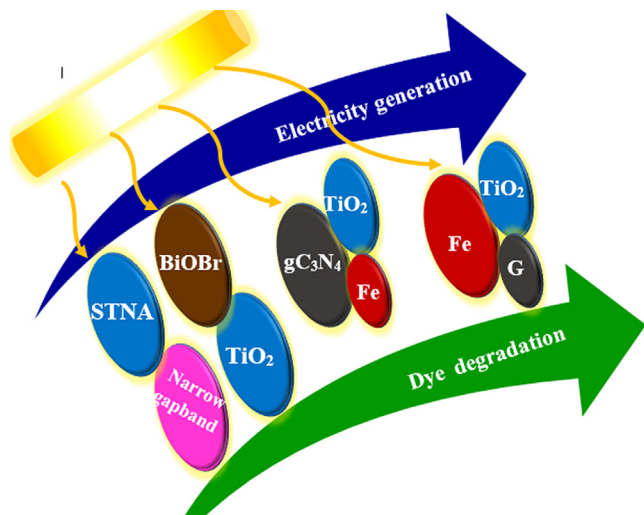

Fig. 4 Effect of different anodic nanocomposite on electricity generation and dye degradation in PFC.

increases the lifetime and improves the quantum performance of the composite catalyst.

However, a more in-depth analysis of the photoanode materials should be more performed. Due to insignificant conductivity characterizations and its photo absorbency in the range of the VLR up to approximately infrared, the photoanode materials with low Eg have led the negligible change of power density, photocurrent and voltage output in the attendance and inexistence of the LR source and pollutant degradation. Moreover, the degradation trend of pollutants is affected by the e^- activity recombination rate and Eg of photoanode materials. In the PFCs, as it maintains the e^- - h^+ pair separation of photoanode, the presence of dissolved oxygen can improve the degradation of pollutants and power generation.

Durability and reusability of photonode is essential for its application in the real world and economic practicality. One method to determine the stability and reusability of electrodes is XRD test. In this regard, XRD test can be applied for fresh and used photoanodes and if the crystalline phase of the photoanode remains constant after several consecutive periods, it can be seen that the used photoanode can be reused and therefore can be used in the wastewater treatment.

Regarding dye removal by PFCs, it can be concluded that the molecular structure of the dyes and LR source significantly influence on dye degradation and power generation. Due to the formation of HO, higher aeration rate, electrolyte pH and degradability of pollutants, as well as a lower concentration of a pollutant in the PFCs, led to an increase of pollutant degradation. However, an increase in resistance leads to reduced pollutant degradation. Furthermore, as raising the LR intensity generates more photo-excited e^-- h^+ pairs, the efficiency is enhanced. The results of the analyzed studies show that PFCs with the membrane electrode assembly structure has a higher pollutant decomposition and simultaneous power generation. Meanwhile, the increase of organic pollutants in the wastewater led to enhance electricity generation.
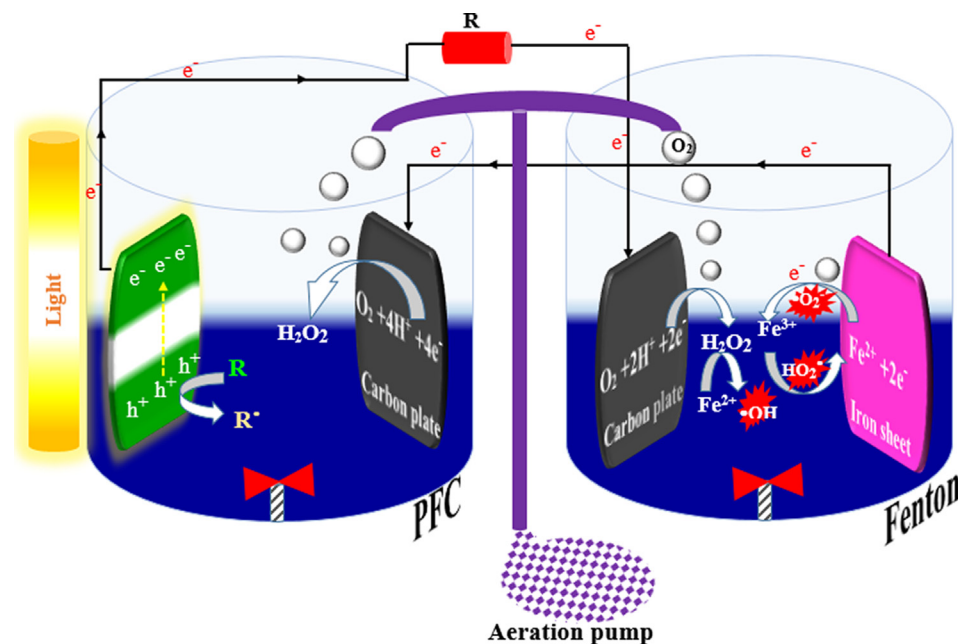

Fig. 5 An example of the hybrid Fenton-PFC system.

In the hybrid PFC-Fenton system, as a result of the introduction of ferrous ions into the PFC to strengthen the radicals' reaction and promote $^{\bullet}OH$ production, the performance of the system was improved for both degradations of pollutant and power production. The use of photoanode and photocathode materials in different forms can lead to an outstanding improvement of both pollutant decomposition and power generation.

Nowadays, the utilization of PFC systems was mostly concentrated on the expansion of high-efficiency photoanode substances, binary photoelectrodes PFCs, and multi-purpose PFCs. Further research work is necessary to improve the performance and economic viability of these systems, the main aspects for each answer are still pending focusing on: i) what is the relevance between the physicochemical characteristics of electrode materials and the performance of related cell?; ii) how can state-of-the-art nanotechnology be combined to further increase the cell yield?; iii) can a PFC device be applied for practical usage?; and iv) how to efficiently employ the generated electricity or H_2? Therefore, these topics are of critical significance for future expansions of any PFC device. Merged approaches that combine advances in theoretical computation and experimental data can supply the needed insights towards the essential related between electrode materials and cell efficiency. This can sufficiently progress the basic knowledge of electrode structures and result in a new strategy of energy generation with practical and efficient real-life use.

Declaration of Competing Interest

The authors declare that they have no known competing financial interests or personal relationships that could have appeared to influence the work reported in this paper.

References

Li, L., Li, J., Bai, J., Zeng, Q., Xia, L., Zhang, Y., Chen, S., Xu, Q., Zhou, B., 2019. The effect and mechanism of organic pollutants oxidation and chemical energy conversion for neutral wastewater via strengthening reactive oxygen species. Sci. Total Environ. 651, 1226–1235.

Liu, Y., Wu, P., Liu, F., Li, F., An, X., Liu, J., Wang, Z., Shen, C., Sand, W., 2019. Electroactive modified carbon nanotube filter for simultaneous detoxification and sequestration of Sb (III). Environ. Sci. Technol. 53, 1527–1535.

Liu, X.-H., Du, F., Chen, Q.-Y., Wang, Y.-H., 2017. An effective self-driven PFC-PEC hybrid system for hydrogen generation from organic substance. Electrochim. Acta 245, 379–385.

Khatri, J., Nidheesh, P., Singh, T.A., Kumar, M.S., 2018. Advanced oxidation processes based on zero-valent aluminium for treating textile wastewater. Chem. Eng. J. 348, 67–73.

Vasseghian, Y., Dragoi, E.-N., 2018. Modeling and optimization of acid blue 193 removal by UV and peroxydisulfate process. J. Environ. Eng. 144, 06018003.

Vasseghian, Y., Moradi, M., Pirsaheb, M., Khataee, A., Rahimi, S., Badi, M.Y., Khaneghah, A.M., 2020. Pesticide decontamination using UV/ferrous-activated persulfate with the aid neuro-fuzzy modeling: a case study of Malathion. Food Res. Int. 137, 109557.

Sarac, M., Ozturk, K., Yatmaz, H., 2020. A facile two-step fabrication of titanium dioxide coated copper oxide nanowires with enhanced photocatalytic performance. Mater. Charact. 159, 110042.

Wang, F., Wu, Y., Wang, Y., Li, J., Jin, X., Zhang, Q., Li, R., Yan, S., Liu, H., Feng, Y., 2019. Construction of novel Z-scheme nitrogen-doped carbon dots/{0 0 1} TiO2 nanosheet photocatalysts for broad-spectrum-driven diclofenac degradation: Mechanism insight, products and effects of natural water matrices. Chem. Eng. J. 356, 857–868.

Jiang, N., Guo, L., Qiu, C., Zhang, Y., Shang, K., Lu, N., Li, J., Wu, Y., 2018. Reactive species distribution characteristics and toluene destruction in the three-electrode DBD reactor energized by different pulsed modes. Chem. Eng. J.

Wang, C., Sun, S., Zhang, L., Yin, J., Jiao, T., Zhang, L., Xu, Y., Zhou, J., Peng, Q., 2019. Facile preparation and catalytic performance characterization of AuNPs-loaded hierarchical electrospun composite fibers by solvent vapor annealing treatment. Colloids Surf., A 561, 283–291.

Li, M., Liu, Y., Dong, L., Shen, C., Li, F., Huang, M., Ma, C., Yang, B., An, X., Sand, W., 2019. Recent advances on photocatalytic fuel cell for environmental applications—the marriage of photocatalysis and fuel cells. Sci. Total Environ. 668, 966–978.

Li, S., Cheng, C., Thomas, A., 2017. Carbon-based microbial-fuel-cell electrodes: from conductive supports to active catalysts. Adv. Mater. 29, 1602547.

Lee, S.-L., Ho, L.-N., Ong, S.-A., Wong, Y.-S., Voon, C.-H., Khalik, W.F., Yusoff, N.A., Nordin, N., 2018. Exploring the relationship between molecular structure of dyes and light sources for photodegradation and electricity generation in photocatalytic fuel cell. Chemosphere 209, 935–943.

Nordin, N., Ho, L.-N., Ong, S.-A., Ibrahim, A.H., Lee, S.-L., Ong, Y.-P., 2019. Elucidating the effects of different photoanode materials on electricity generation and dye degradation in a sustainable hybrid system of photocatalytic fuel cell and peroxi-coagulation process. Chemosphere 214, 614–622.

Lee, S.-L., Ho, L.-N., Ong, S.-A., Wong, Y.-S., Voon, C.-H., Khalik, W.F., Yusoff, N.A., Nordin, N., 2018. Role of dissolved oxygen on the degradation mechanism of Reactive Green 19 and electricity generation in photocatalytic fuel cell. Chemosphere 194, 675–681.

Ong, Y.-P., Ho, L.-N., Ong, S.-A., Banjuraizah, J., Ibrahim, A.H., Lee, S.-L., Nordin, N., 2019. A synergistic heterostructured ZnO/BaTiO3 loaded carbon photoanode in photocatalytic fuel cell for degradation of Reactive Red 120 and electricity generation. Chemosphere 219, 277–285.

Khalik, W.F., Ho, L.-N., Ong, S.-A., Voon, C.-H., Wong, Y.-S., Yusoff, N., Lee, S.-L., Yusuf, S.Y., 2017. Optimization of degradation of Reactive Black 5 (RB5) and electricity generation in solar photocatalytic fuel cell system. Chemosphere 184, 112–119.

Tang, S., Li, N., Yuan, D., Tang, J., Li, X., Zhang, C., Rao, Y., 2019. Comparative study of persulfate oxidants promoted photocatalytic fuel cell performance: simultaneous dye removal and electricity generation. Chemosphere 234, 658–667.

Li, N., Tang, S., Rao, Y., Qi, J., Zhang, Q., Yuan, D., 2019. Peroxymonosulfate enhanced antibiotic removal and synchronous electricity generation in a photocatalytic fuel cell. Electrochim. Acta 298, 59–69.

Zhao, K., Bai, J., Zeng, Q., Zhang, Y., Li, J., Li, L., Xia, L., Zhou, B., 2017. Efficient wastewater treatment and simultaneously electricity production using a photocatalytic fuel cell based on the radical chain reactions initiated by dual photoelectrodes. J. Hazard. Mater. 337, 47–54.

Deng, B., Fu, S., Zhang, Y., Wang, Y., Ma, D., Dong, S., 2018. Simultaneous pollutant degradation and power generation in visible-light responsive photocatalytic fuel cell with an Ag-TiO2 loaded photoanode. Nano-Struct. Nano-Objects 15, 167–172.

Lu, Y., Chu, Y., Zheng, W., Huo, M., Huo, H., Qu, J., Yu, H., Zhao, Y., 2019. Significant tetracycline hydrochloride degradation and electricity generation in a visible-light-driven dual photoelectrode photocatalytic fuel cell using BiVO4/TiO2 NT photoanode and Cu2O/TiO2 NT photocathode. Electrochim. Acta 320, 134617.

Wang, D., Li, Y., Puma, G.L., Lianos, P., Wang, C., Wang, P., 2017. Photoelectrochemical cell for simultaneous electricity generation and heavy metals recovery from wastewater. J. Hazard. Mater. 323, 681–689.

Xia, M., Chen, R., Zhu, X., Liao, Q., An, L., Wang, Z., He, X., Jiao, L., 2016. A micro photocatalytic fuel cell with an air-breathing, membraneless and monolithic design. Sci. Bull. 61, 1699–1710.

Sfaelou, S., Sygellou, L., Dracopoulos, V., Travlos, A., Lianos, P., 2014. Effect of the nature of cadmium salts on the effectiveness of CdS SILAR deposition and its consequences on the performance of sensitized solar cells. J. Phys. Chem. C 118, 22873–22880.

Fang, Z., Song, H., Yu, R., Li, X., 2016. A microbial fuel cell-coupled constructed wetland promotes degradation of azo dye decolorization products. Ecol. Eng. 94, 455–463.

Wu, C., Liu, L., Tang, K., Chen, T., 2017. Studies on an ultrasonic atomization feed direct methanol fuel cell. Ultrason. Sonochem. 34, 60–66.

Qi, J., Ge, J., Uddin, M.A., Zhai, Y., Pasaogullari, U., St-Pierre, J., 2018. Evaluation of cathode contamination with Ca2 + in proton exchange membrane fuel cells. Electrochim. Acta 259, 510–516.

Lan, C., Fang, J., Guan, Y., Zhou, H., Zhao, J., 2015. Cross-linked anion exchange membranes with pendent quaternary pyrrolidonium salts for alkaline polymer electrolyte membrane fuel cells. J. Power Sources 295, 259–267.

Kee, M.W., Soo, J.W., Lam, S.M., Sin, J.C., Mohamed, A.R., 2018. Evaluation of photocatalytic fuel cell (PFC) for electricity production and simultaneous degradation of methyl green in synthetic and real greywater effluents. J. Environ. Manage. 228, 383–392.

Das, R., Vecitis, C.D., Schulze, A., Cao, B., Ismail, A.F., Lu, X., Chen, J., Ramakrishna, S., 2017. Recent advances in nanomaterials for water protection and monitoring. Chem. Soc. Rev. 46, 6946–7020.

Xiang, Q., Yu, J., Jaroniec, M., 2012. Graphene-based semiconductor photocatalysts. Chem. Soc. Rev. 41, 782–796.

Martin, D.J., Liu, G., Moniz, S.J., Bi, Y., Beale, A.M., Ye, J., Tang, J., 2015. Efficient visible driven photocatalyst, silver phosphate: performance, understanding and perspective. Chem. Soc. Rev. 44, 7808–7828.

Li, K., Zhang, H., Tang, T., Xu, Y., Ying, D., Wang, Y., Jia, J., 2014. Optimization and application of TiO2/Ti–Pt photo fuel cell (PFC) to effectively generate electricity and degrade organic pollutants simultaneously. Water Res. 62, 1–10.

Khataee, A., Fathinia, M., Zarei, M., Izadkhah, B., Joo, S., 2014. Modeling and optimization of photocatalytic/photoassisted-electro-Fenton like degradation of phenol using a neural network coupled with genetic algorithm. J. Ind. Eng. Chem. 20, 1852–1860.

Ying, D., Cao, R., Li, C., Tang, T., Li, K., Wang, H., Wang, Y., Jia, J., 2016. Study of the photocurrent in a photocatalytic fuel cell for wastewater treatment and the effects of TiO2 surface morphology to the apportionment of the photocurrent. Electrochim. Acta 192, 319–327.

Antoniadou, M., Daskalaki, V.M., Balis, N., Kondarides, D.I., Kordulis, C., Lianos, P., 2011. Photocatalysis and photoelectrocatalysis using (CdS-ZnS)/TiO2 combined photocatalysts. Appl. Catal. B 107, 188–196.

Liu, Y., Liu, L., Yang, F., 2016. Energy-efficient degradation of rhodamine B in a LED illuminated photocatalytic fuel cell with anodic Ag/AgCl/GO and cathodic ZnIn 2 S 4 catalysts. RSC Adv. 6, 12068–12075.

Xie, S., Ouyang, K., 2017. Degradation of refractory organic compounds by photocatalytic fuel cell with solar responsive WO3/FTO photoanode and air-breathing cathode. J. Colloid Interface Sci. 500, 220–227.

Lee, S.-L., Ho, L.-N., Ong, S.-A., Wong, Y.-S., Voon, C.-H., Khalik, W.F., Yusoff, N.A., Nordin, N., 2017. A highly efficient immobilized ZnO/Zn photoanode for degradation of azo dye Reactive Green 19 in a photocatalytic fuel cell. Chemosphere 166, 118–125.

Xie, S., Ouyang, K., Shao, Y., 2017. A solar responsive photocatalytic fuel cell with a heterostructured ZnFe2O4/TiO2-NTs photoanode and an air-breathing cathode. Int. J. Hydrogen Energy 42, 29201–29209.

Zeng, Q., Bai, J., Li, J., Li, L., Xia, L., Zhou, B., Sun, Y., 2018. Highly-stable and efficient photocatalytic fuel cell based on an epitaxial TiO 2/WO 3/W nanothorn photoanode and enhanced radical reactions for simultaneous electricity production and wastewater treatment. Appl. Energy 220, 127–137.

Ye, Y., Bruning, H., Li, X., Yntema, D., Rijnaarts, H.H., 2018. Significant enhancement of micropollutant photocatalytic degradation using a TiO2 nanotube array photoanode based photocatalytic fuel cell. Chem. Eng. J. 354, 553–562.

Iqbal, M., Thebo, A.A., Shah, A.H., Iqbal, A., Thebo, K.H., Phulpoto, S., Mohsin, M.A., 2017. Influence of Mn-doping on the photocatalytic and solar cell efficiency of CuO nanowires. Inorg. Chem. Commun. 76, 71–76.

Xie, S., Lu, X., Zhai, T., Gan, J., Li, W., Xu, M., Yu, M., Zhang, Y.-M., Tong, Y., 2012. Controllable synthesis of Zn x Cd1–x S@ ZnO core-shell nanorods with enhanced photocatalytic activity. Langmuir 28, 10558–10564.

Yang, Y., Zhang, W., Liu, R., Cui, J., Deng, C., 2018. Preparation and photocatalytic properties of visible light driven Ag-AgBr-RGO composite. Sep. Purif. Technol. 190, 278–287.

Hailili, R., Wang, Z.-Q., Li, Y., Wang, Y., Sharma, V.K., Gong, X.-Q., Wang, C., 2018. Oxygen vacancies induced visible-light photocatalytic activities of CaCu3Ti4O12 with controllable morphologies for antibiotic degradation. Appl. Catal. B 221, 422–432.

Osouleddini, N., Tajik, L., Moradi, M., 2019. Degradation of amoxicillin by persulfate activated with Fe3O4/GO nanocomposite in aqueous solution. Desalin. Water Treat. 153, 392–401.

Zarei, M., Khataee, A., Fathinia, M., Seyyednajafi, F., Ranjbar, H., 2012. Combination of nanophotocatalysis with electro-Fenton-like process in the removal of phenol from aqueous solution: GC analysis and response surface approach. Int. J. Indus. Chem. 3, 27.

Alikarami, M., Soltani, R.D.C., Khataee, A., 2019. An innovative combination of electrochemical and photocatalytic processes for decontamination of bisphenol A endocrine disruptor form aquatic phase: Insight into mechanism, enhancers and bio-toxicity assay. Sep. Purif. Technol. 220, 42–51.

Khataee, A., Zarei, M., Ordikhani-Seyedlar, R., 2011. Heterogeneous photocatalysis of a dye solution using supported TiO2 nanoparticles combined with homogeneous photoelectrochemical process: molecular degradation products. J. Mol. Catal. A: Chem. 338, 84–91.

Katsumata, H., Taniguchi, M., Kaneco, S., Suzuki, T., 2013. Photocatalytic degradation of bisphenol A by Ag3PO4 under visible light. Catal. Commun. 34, 30–34.

Chen, Q., Bai, J., Li, J., Huang, K., Li, X., Zhou, B., Cai, W., 2014. Aerated visible-light responsive photocatalytic fuel cell for wastewater treatment with producing sustainable electricity in neutral solution. Chem. Eng. J. 252, 89–94.

Tang, T., Li, K., Ying, D., Sun, T., Wang, Y., Jia, J., 2014. High efficient aqueous-film rotating disk photocatalytic fuel cell (RDPFC) with triple functions: cogeneration of hydrogen and electricity with dye degradation, international journal of hydrogen energy 39 (2014) 10258–10266.

Wu, Z., Zhao, G., Zhang, Y., Liu, J., Zhang, Y.-N., Shi, H., 2015. A solar-driven photocatalytic fuel cell with dual photoelectrode for simultaneous wastewater treatment and hydrogen production. J. Mater. Chem. A 3, 3416–3424.

Yang, C., He, Y., Li, K., Yao, Y., Cao, R., Wang, Y., Jia, J., 2015. Degrading organic pollutants and generating electricity in a dual-chamber rotating-disk photocatalytic fuel cell (RPFC) with a TiO2 nanotube array anode. Res. Chem. Intermed. 41, 5365–5377.

Bai, J., Wang, R., Li, Y., Tang, Y., Zeng, Q., Xia, L., Li, X., Li, J., Li, C., Zhou, B., 2016. A solar light driven dual photoelectrode photocatalytic fuel cell (PFC) for simultaneous wastewater treatment and electricity generation. J. Hazard. Mater. 311, 51–62.

Lee, S.-L., Ho, L.-N., Ong, S.-A., Wong, Y.-S., Voon, C.-H., Khalik, W.F., Yusoff, N.A., Nordin, N., 2016. Enhanced electricity

generation and degradation of the azo dye Reactive Green 19 in a photocatalytic fuel cell using ZnO/Zn as the photoanode. J. Cleaner Prod. 127, 579–584.

Shen, Z., Wu, D., Yang, J., Yuan, T., Wang, W., Jia, J., 2006. Methods to improve electrochemical treatment effect of dye wastewater. J. Hazard. Mater. 131, 90–97.

Saquib, M., Muneer, M., 2003. TiO2-mediated photocatalytic degradation of a triphenylmethane dye (gentian violet), in aqueous suspensions. Dyes Pigm. 56, 37–49.

Saquib, M., Muneer, M., 2003. Photocatalytic degradation of two selected textile dye derivatives, eosine yellowish and p-rosaniline, in aqueous suspensions of titanium dioxide. J. Environ. Sci. Health, Part A 38, 2581–2598.

Sui, M., Dong, Y., Wang, Z., Wang, F., You, H., 2017. A biocathode-driven photocatalytic fuel cell using an Ag-doped TiO2/Ti mesh photoanode for electricity generation and pollutant degradation. J. Photochem. Photobiol., A 348, 238–245.

Zhao, K., Zeng, Q., Bai, J., Li, J., Xia, L., Chen, S., Zhou, B., 2017. Enhanced organic pollutants degradation and electricity production simultaneously via strengthening the radicals reaction in a novel Fenton-photocatalytic fuel cell system. Water Res. 108, 293–300.

Li, N., Tang, S., Rao, Y., Qi, J., Wang, P., Jiang, Y., Huang, H., Gu, J., Yuan, D., 2018. Improved dye removal and simultaneous electricity production in a photocatalytic fuel cell coupling with persulfate activation. Electrochim. Acta 270, 330–338.

Lu, L., Jiang, T., Jing, W.-S., Zhou, G.-W., Shi, H.-X., 2018. A Visible light responsive photocatalytic fuel cell using BiOBr/TiO2 nanotube array photoanode for simultaneous wastewater treatment and electricity generation. Chem. Lett. 47, 613–616.

Sharma, J., Mishra, I., Dionysiou, D.D., Kumar, V., 2015. Oxidative removal of bisphenol A by UV-C/peroxymonosulfate (PMS): kinetics, influence of co-existing chemicals and degradation pathway. Chem. Eng. J. 276, 193–204.

Chen, J., Fang, C., Xia, W., Huang, T., Huang, C.-H., 2018. Selective transformation of β-lactam antibiotics by peroxymonosulfate: reaction kinetics and nonradical mechanism. Environ. Sci. Technol. 52, 1461–1470.

Yang, Y., Banerjee, G., Brudvig, G.W., Kim, J.-H., Pignatello, J.J., 2018. Oxidation of organic compounds in water by unactivated peroxymonosulfate. Environ. Sci. Technol. 52, 5911–5919.

Sayed, M., Khan, J.A., Shah, L.A., Shah, N.S., Shah, F., Khan, H. M., Zhang, P., Arandiyan, H., 2017. Solar light responsive poly (vinyl alcohol)-assisted hydrothermal synthesis of immobilized TiO2/Ti film with the addition of peroxymonosulfate for photocatalytic degradation of ciprofloxacin in aqueous media: a mechanistic approach. J. Phys. Chem. C 122, 406–421.

Chen, Q., Li, J., Li, X., Huang, K., Zhou, B., Cai, W., Shangguan, W., 2012. Visible-light responsive photocatalytic fuel cell based on WO3/W photoanode and Cu2O/Cu photocathode for simultaneous wastewater treatment and electricity generation. Environ. Sci. Technol. 46, 11451–11458.

Li, L., Wang, G., Chen, R., Zhu, X., Wang, H., Liao, Q., Yu, Y., 2014. Optofluidics based micro-photocatalytic fuel cell for efficient wastewater treatment and electricity generation. Lab Chip 14, 3368–3375.

Khalik, W.F., Ong, S.-A., Ho, L.-N., Wong, Y.-S., Voon, C.-H., Yusuf, S.Y., Yusoff, N.A., Lee, S.-L., 2016. Influence of supporting electrolyte in electricity generation and degradation of organic pollutants in photocatalytic fuel cell. Environ. Sci. Pollut. Res. 23, 16716–16721.

Sui, M., Dong, Y., Bai, W., Ambuchi, J.J., You, H., 2017. In-situ utilization of generated electricity in a photocatalytic fuel cell to enhance pollutant degradation. J. Photochem. Photobiol., A 343, 51–57.

Mousavi, S.A., Vasseghian, Y., Bahadori, A., 2020. Evaluate the performance of Fenton process for the removal of Methylene Blue from aqueous solution: experimental, neural network modeling and optimization. Environ. Prog. Sustainable Energy 39 (2), 1–7.

Nahyoon, N.A., Liu, L., Rabe, K., Thebo, K.H., Yuan, L., Sun, J., Yang, F., 2018. Significant photocatalytic degradation and electricity generation in the photocatalytic fuel cell (PFC) using novel anodic nanocomposite of Fe, graphene oxide, and titanium phosphate. Electrochim. Acta 271, 41–48.

Rabé, K., Liu, L., Nahyoon, N.A., Zhang, Y., Idris, A.M., 2019. Visible-light photocatalytic fuel cell with Z-scheme g-C3N4/Fe0/TiO2 anode and WO3 cathode efficiently degrades berberine chloride and stably generates electricity. Sep. Purif. Technol. 212, 774–782.

Wang, Y., Lan, Y., Bu, D., Qian, B., Wang, Y., Wang, B., Wu, Q., Li, S., Zhang, Y., Song, X.-M., 2020. A study on tandem photoanode and photocathode for photocatalytic formaldehyde fuel cell. Electrochim. Acta 136476.

Yu, H., Xue, Y., Lu, Y., Wang, X., Zhu, S., Qin, W., Huo, M., 2020. Novel application of a Z-scheme photocatalyst of Ag3PO4@ g-C3N4 for photocatalytic fuel cells. J. Environ. Manage. 254, 109738.

Lam, S.-M., Sin, J.-C., Lin, H., Li, H., Zeng, H., 2020. Greywater and bacteria removal with synchronized energy production in photocatalytic fuel cell based on anodic TiO2/ZnO/Zn and cathodic CuO/Cu. Chemosphere 245, 125565.

Chen, X., Yao, J., Xia, B., Gan, J., Gao, N., Zhang, Z., 2020. Influence of pH and DO on the ofloxacin degradation in water by UVA-LED/TiO2 nanotube arrays photocatalytic fuel cell: mechanism, ROSs contribution and power generation. J. Hazard. Mater. 383, 121220.

Lam, S.-M., Sin, J.-C., Hua, L., Haixiang, L., Wei, L.J., Zeng, H., 2020. A Z-scheme WO3 loaded-hexagonal rod-like ZnO/Zn photocatalytic fuel cell for chemical energy recuperation from food wastewater treatment. Appl. Surf. Sci. 145945.

Kee, M.-W., Lam, S.-M., Sin, J.-C., Zeng, H., Mohamed, A.R., 2020. Explicating charge transfer dynamics in anodic TiO2/ZnO/Zn photocatalytic fuel cell for ameliorated palm oil mill effluent treatment and synchronized energy generation. J. Photochem. Photobiol., A 391, 112353.

Zhang, J., Dong, S., Zhang, X., Zhu, S., Zhou, D., Crittenden, J.C., 2018. Photocatalytic removal organic matter and bacteria simultaneously from real WWTP effluent with power generation concomitantly: using an ErAlZnO photo-anode. Sep. Purif. Technol. 191, 101–107.

Ren, J., Wang, W., Zhang, L., Chang, J., Hu, S., 2009. Photocatalytic inactivation of bacteria by photocatalyst Bi2WO6 under visible light. Catal. Commun. 10, 1940–1943.

Matsunaga, T., Tomoda, R., Nakajima, T., Wake, H., 1985. Photoelectrochemical sterilization of microbial cells by semiconductor powders. FEMS Microbiol. Lett. 29, 211–214.

Yu, J.C., Ho, W., Yu, J., Yip, H., Wong, P.K., Zhao, J., 2005. Efficient visible-light-induced photocatalytic disinfection on sulfur-doped nanocrystalline titania. Environ. Sci. Technol. 39, 1175–1179.

Elahifard, M.R., Rahimnejad, S., Haghighi, S., Gholami, M.R., 2007. Apatite-coated Ag/AgBr/TiO2 visible-light photocatalyst for destruction of bacteria. J. Am. Chem. Soc. 129, 9552–9553.

Wang, W., Zeng, Z., Zeng, G., Zhang, C., Xiao, R., Zhou, C., Xiong, W., Yang, Y., Lei, L., Liu, Y., 2019. Sulfur doped carbon quantum dots loaded hollow tubular g-C3N4 as novel photocatalyst for destruction of Escherichia coli and tetracycline degradation under visible light. Chem. Eng. J. 378, 122132.

Shanmugam, V., Jeyaperumal, K.S., Mariappan, P., Muppudathi, A. L., 2020. Fabrication of novel g-C3N4 based MoS2 and Bi2O3 nanorods embedded ternary nanocomposites for superior photocatalytic performance and destruction of bacteria. New J. Chem.

Lianos, P., 2017. Review of recent trends in photoelectrocatalytic conversion of solar energy to electricity and hydrogen. Appl. Catal. B 210, 235–254.

Sfaelou, S., Lianos, P., 2016. Photoactivated Fuel Cells (Photo-FuelCells). An alternative source of renewable energy with environmental benefits. AIMS Mater. Sci. 3, 270–288.

Xia, L., Bai, J., Li, J., Zeng, Q., Li, X., Zhou, B., 2016. A highly efficient BiVO4/WO3/W heterojunction photoanode for visible-light responsive dual photoelectrode photocatalytic fuel cell. Appl. Catal. B 183, 224–230.

Lianos, P., 2011. Production of electricity and hydrogen by photocatalytic degradation of organic wastes in a photoelectrochemical cell: the concept of the photofuelcell: a review of a re-emerging research field. J. Hazard. Mater. 185, 575–590.

Varghese, O.K., Grimes, C.A., 2008. Appropriate strategies for determining the photoconversion efficiency of water photoelectrolysis cells: a review with examples using titania nanotube array photoanodes. Sol. Energy Mater. Sol. Cells 92, 374–384.

Antoniadou, M., Kondarides, D.I., Dionysiou, D.D., Lianos, P., 2012. Quantum dot sensitized titania applicable as photoanode in photoactivated fuel cells. The Journal of Physical Chemistry C 116, 16901–16909.

B. O'regan, M. Grätzel, A low-cost, high-efficiency solar cell based on dye-sensitized colloidal TiO2 films, nature 353 (1991) 737.

Liu, Y., Li, J., Zhou, B., Li, X., Chen, H., Chen, Q., Wang, Z., Li, L., Wang, J., Cai, W., 2011. Efficient electricity production and simultaneously wastewater treatment via a high-performance photocatalytic fuel cell. Water Res. 45, 3991–3998.

Li, K., Xu, Y., He, Y., Yang, C., Wang, Y., Jia, J., 2013. Photocatalytic fuel cell (PFC) and dye self-photosensitization photocatalytic fuel cell (DSPFC) with BiOCl/Ti photoanode under UV and visible light irradiation. Environ. Sci. Technol. 47, 3490–3497.

Li, L., Xue, S., Chen, R., Liao, Q., Zhu, X., Wang, Z., He, X., Feng, H., Cheng, X., 2015. Performance characteristics of a membrane-less solar responsive photocatalytic fuel cell with an air-breathing cathode under different fuels and electrolytes and air conditions. Electrochim. Acta 182, 280–288.

Yang, J., Liao, W., Liu, Y., Murugananthan, M., Zhang, Y., 2014. Degradation of Rhodamine B using a visible-light driven photocatalytic fuel cell. Electrochim. Acta 144, 7–15.

Zuorro, A., Roberto, L., 2014. Evaluation of UV/H2O2 advanced oxidation process (AOP) for the degradation of diazo dye Reactive Green 19 in aqueous solution. Desalin. Water Treat. 52, 1571–1577.

Pan, H., Wenjuan, L., Na, S., Muthu, M., Yanrong, Z., 2018. Highly efficient and visible light responsive heterojunction composites as dual photoelectrodes for photocatalytic fuel cell. Catalysts 8, 30.

Tada, H., Tomohiro, M., Tomokazu, K., Tomoki, A., Koji, T., 2006. All-solid-state Z-scheme in CdS–Au–TiO 2 three-component nanojunction system. Nat. Mater. 5, 782.

Maeda, K., 2013. Z-scheme water splitting using two different semiconductor photocatalysts. ACS Catal. 3, 1486–1503.

Zhou, P., Jiaguo, Y., Mietek, J., 2014. All-solid-state Z-scheme photocatalytic systems. Adv. Mater. 26, 4920–4935.

Fujishima, A., Kenichi, H., 1972. Electrochemical photolysis of water at a semiconductor electrode. Nature 238, 37.

Darbandi, M., Shaabani, B., Schneider, J., Bahnemann, D., Gholami, P., Khataee, A., Yardani, P., Hosseini, M.G., 2019. TiO2 nanoparticles with superior hydrogen evolution and pollutant degradation performance. Int. J. Hydrogen Energy 44, 24162–24173.

Veziroğlu, T.N., 2008. IJHE mobilizes to reach hydrogen civilization. Int. J. Hydrogen Energy 1, 1–2.

M.A. Ruiz-Gómez, T.-M. Leticia M., F.-T. Mayra Z., M. Edgar, J.-R. Isaías, Hydrogen evolution from pure water over a new advanced photocatalyst Sm2GaTaO7, international journal of hydrogen energy 38 (2013) 12554-12561.

Kelly, N.A., G. Thomas L., Solar energy concentrating reactors for hydrogen production by photoelectrochemical water splitting, International Journal of Hydrogen Energy 33 (2008) 6420–6431.

Michal, R., Stavroula, S., Panagiotis, L., 2014. Photocatalysis for renewable energy production using PhotoFuelCells. Molecules 19, 19732–19750.

Papagiannis, I., Stathi, P., Deligiannakis, Y., Keramidas, A., Lianos, P., 2020. Photoelectrocatalytic production of hydrogen peroxide using a photo (catalytic) fuel cell. J. Photochem. Photobiol., A 389, 112210.

Chiarello, G.L., Aguirre, M.H., Elena, S., 2010. Hydrogen production by photocatalytic steam reforming of methanol on noble metal-modified TiO2. J. Catal. 273, 182–190.

Nomikos, G.N., Paraskevi, P., Kondarides, D.I., Verykios, X.E., 2014. Kinetic and mechanistic study of the photocatalytic reforming of methanol over Pt/TiO2 catalyst. Appl. Catal. B 146, 249–257.

Li, Z., Wenjun, L., Minglong, Z., Jianyong, F., Zhigang, Z., 2013. Photoelectrochemical cells for solar hydrogen production: current state of promising photoelectrodes, methods to improve their properties, and outlook. Energy Environ. Sci. 6, 347–370.

Kim, J.H., Hiroyuki, K., Tsutomu, M., Jun, K., Kazunari, D., Lee, J.S., 2016. Overall photoelectrochemical water splitting using tandem cell under simulated sunlight. ChemSusChem 9, 61–66.

Khan, S.U., Mofareh, A.-S., Ingler, W.B., 2002. Efficient photochemical water splitting by a chemically modified n-TiO2, Science 297 (2002) 2243–2245.

Lin, C.J., Shu-Jun, L., Li-Cheng, K., Liou, S.Y.H., 2015. Photoelectrocatalytic activity of a hydrothermally grown branched Zno nanorod-array electrode for paracetamol degradation. J. Hazard. Mater. 291, 9–17.

Wang, M., Lan, S., Zhiqun, L., Jianhuai, C., Kunpeng, X., Lin, C., 2013. p–n Heterojunction photoelectrodes composed of Cu2O-loaded TiO2 nanotube arrays with enhanced photoelectrochemical and photoelectrocatalytic activities. Energy Environ. Sci. 6, 1211–1220.

Huang, W.-C., Lyu, L.-M., Yang, Y.-C., Huang, M.H., 2011. Synthesis of Cu2O nanocrystals from cubic to rhombic dodecahedral structures and their comparative photocatalytic activity. J. Am. Chem. Soc. 134, 1261–1267.

Venkatkarthick, R., Davidson, D.J., Vasudevan, S., Sozhan, G., Ravichandran, S., 2017. An investigation of interfacial and photoelectrochemical performance of thermally prepared C, N-codoped TiO2 photoanodes for water splitting. ChemistrySelect 2, 288–294.

Venkatkarthick, R., Kiruthika, G.V.M., Davidson, D.J., Ravichandran, S., Sozhan, G., Vasudevan, S., 2016. New insight into understand the enhanced photoconductivity properties of Ti (O2) plate spurted with Al2O3 for water oxidation. ChemistrySelect 1, 5037–5041.

Ong, C.B., Ng, L.Y., Mohammad, A.W., 2018. A review of ZnO nanoparticles as solar photocatalysts: synthesis, mechanisms and applications. Renew. Sustain. Energy Rev. 81, 536–551.

Strataki, N., Antoniadou, M., Dracopoulos, V., Lianos, P., 2010. Visible-light photocatalytic hydrogen production from ethanol–water mixtures using a Pt–CdS–TiO2 photocatalyst. Catal. Today 151, 53–57.

Monfort, O., Pop, L.-C., Sfaelou, S., Plecenik, T., Roch, T., Dracopoulos, V., Stathatos, E., Plesch, G., Lianos, P., 2016. Photoelectrocatalytic hydrogen production by water splitting using BiVO4 photoanodes. Chem. Eng. J. 286, 91–97.

Gan, J., Lu, X., Tong, Y., 2014. Towards highly efficient photoanodes: boosting sunlight-driven semiconductor nanomaterials for water oxidation. Nanoscale 6, 7142–7164.

Horiuchi, Y., Toyao, T., Takeuchi, M., Matsuoka, M., Anpo, M., 2013. Recent advances in visible-light-responsive photocatalysts for hydrogen production and solar energy conversion–from semiconducting TiO 2 to MOF/PCP photocatalysts. PCCP 15, 13243–13253.

Bhatt, M.D., Lee, J.S., 2015. Recent theoretical progress in the development of photoanode materials for solar water splitting

photoelectrochemical cells. J. Mater. Chem. A 3, 10632–10659.

Pirsaheb, M., Karimi, K., Shahmoradi, B., Moradi, M., Vasseghian, Y., Dragoi, E.N., 2019. Photocatalyzed degradation of acid orange 7 dye under sunlight and ultraviolet irradiation using Ni-doped ZnO nanoparticles. Desalin. Water Treat. 165, 321–332.

Pop, L.-C., Dracopoulos, V., Lianos, P., 2015. Photoelectrocatalytic hydrogen production using nanoparticulate titania and a novel Pt/Carbon electrocatalyst: the concept of the "Photoelectrocatalytic Leaf". Appl. Surf. Sci. 333, 147–151.

Gao, P., Grätzel, M., Nazeeruddin, M.K., 2014. Organohalide lead perovskites for photovoltaic applications. Energy Environ. Sci. 7, 2448–2463.

Alexander, B.D., Kulesza, P.J., Rutkowska, I., Solarska, R., Augustynski, J., 2008. Metal oxide photoanodes for solar hydrogen production. J. Mater. Chem. 18, 2298–2303.

Kaneko, M., Nemoto, J., Ueno, H., Gokan, N., Ohnuki, K., Horikawa, M., Saito, R., Shibata, T., 2006. Photoelectrochemical reaction of biomass and bio-related compounds with nanoporous TiO$_2$ film photoanode and O$_2$-reducing cathode. Electrochem. Commun. 8, 336–340.

Seger, B., Lu, G.Q.M., Wang, L., 2012. Electrical power and hydrogen production from a photo-fuel cell using formic acid and other single-carbon organics. J. Mater. Chem. 22, 10709–10715.

Antoniadou, M., Lianos, P., 2010. Production of electricity by photoelectrochemical oxidation of ethanol in a PhotoFuelCell. Appl. Catal. B 99, 307–313.

Liu, Y., Li, J., Zhou, B., Lv, S., Li, X., Chen, H., Chen, Q., Cai, W., 2012. Photoelectrocatalytic degradation of refractory organic compounds enhanced by a photocatalytic fuel cell. Appl. Catal. B 111, 485–491.

Liu, Y., Li, J., Zhou, B., Chen, H., Wang, Z., Cai, W., 2011. A TiO$_2$-nanotube-array-based photocatalytic fuel cell using refractory organic compounds as substrates for electricity generation. Chem. Commun. 47, 10314–10316.

Li, J., Jinhua, L., Quanpeng, C., Jing, B., Baoxue, Z., 2013. Converting hazardous organics into clean energy using a solar responsive dual photoelectrode photocatalytic fuel cell. J. Hazard. Mater. 262, 304–310.

Wang, H., Zhang, L., Chen, Z., Hu, J., Li, S., Wang, Z., Liu, J., Wang, X., 2014. Semiconductor heterojunction photocatalysts: design, construction, and photocatalytic performances. Chem. Soc. Rev. 43, 5234–5244.

Hashimoto, K., Irie, H., Fujishima, A., 2005. TiO$_2$ photocatalysis: a historical overview and future prospects. Jpn. J. Appl. Phys. 44, 8269.

Paulose, M., Prakasam, H.E., Varghese, O.K., Peng, L., Popat, K.C., Mor, G.K., Desai, T.A., Grimes, C.A., 2007. TiO2 nanotube arrays of 1000 μm length by anodization of titanium foil: phenol red diffusion. J. Phys. Chem. C 111, 14992–14997.

Kim, D.H., Han, G.S., Seong, W.M., Lee, J.W., Kim, B.J., Park, N.G., Hong, K.S., Lee, S., Jung, H.S., 2015. Niobium doping effects on TiO2 mesoscopic electron transport layer-based perovskite solar cells. ChemSusChem 8, 2392–2398.

Li, X., Zheng, W., Pan, H., Yu, Y., Chen, L., Wu, P., 2013. Pt nanoparticles supported on highly dispersed TiO2 coated on SBA-15 as an efficient and recyclable catalyst for liquid-phase hydrogenation. J. Catal. 300, 9–19.

Jiao, Z., Zhang, Y., Chen, T., Dong, Q., Lu, G., Bi, Y., 2014. TiO2 Nanotube arrays modified with Cr-doped SrTiO3 nanocubes for highly efficient hydrogen evolution under visible light, chemistry–A. Eur. J. 20, 2654–2662.

Pang, Y.L., Lim, S., Ong, H.C., Chong, W.T., 2014. A critical review on the recent progress of synthesizing techniques and fabrication of TiO2-based nanotubes photocatalysts. Appl. Catal. A 481, 127–142.

Kaneko, M., Gokan, N., Katakura, N., Takei, Y., Hoshino, M., 2005. Artificial photochemical nitrogen cycle to produce nitrogen and hydrogen from ammonia by platinized TiO 2 and its application to a photofuel cell. Chem. Commun. 12, 1625–1627.

Panagiotopoulou, P., Antoniadou, M., Kondarides, D.I., Lianos, P., 2010. Aldol condensation products during photocatalytic oxidation of ethanol in a photoelectrochemical cell. Appl. Catal. B 100, 124–132.

Antoniadou, M., Kondarides, D.., Labou, D., Neophytides, S., Lianos, P., 2010. An efficient photoelectrochemical cell functioning in the presence of organic wastes. Sol. Energy Mater. Sol. Cells 94, 592–597.

Cao, J., Ji, Y., Tian, C., Yi, Z., 2014. Synthesis and enhancement of visible light activities of nitrogen-doped BaTiO3. J. Alloy. Compd. 615, 243–248.

Liu, J., Sun, Y., Li, Z., 2012. Ag loaded flower-like BaTiO 3 nanotube arrays: Fabrication and enhanced photocatalytic property. CrystEngComm 14, 1473–1478.

Cui, Y., Briscoe, J., Dunn, S., 2013. Effect of ferroelectricity on solar-light-driven photocatalytic activity of BaTiO$_3$ – influence on the carrier separation and stern layer formation. Chem. Mater. 25, 4215–4223.

Sui, M., Dong, Y., You, H., 2015. Enhanced photocatalytic activity for the degradation of rhodamine B by integrating salinity gradient power into a photocatalytic fuel cell. RSC Adv. 5, 94184–94190.

He, X., Chen, M., Chen, R., Zhu, X., Liao, Q., Ye, D., Zhang, B., Zhang, W., Yu, Y., 2018. A solar responsive photocatalytic fuel cell with the membrane electrode assembly design for simultaneous wastewater treatment and electricity generation. J. Hazard. Mater. 358, 346–354.

Jun, H., Im, B., Kim, J.Y., Im, Y.-O., Jang, J.-W., Kim, E.S., Kim, J.Y., Kang, H.J., Hong, S.J., Lee, J.S., 2012. Photoelectrochemical water splitting over ordered honeycomb hematite electrodes stabilized by alumina shielding. Energy Environ. Sci. 5, 6375–6382.

Wang, B., Zhang, H., Lu, X.-Y., Xuan, J., Leung, M.K., 2014. Solar photocatalytic fuel cell using CdS–TiO2 photoanode and air-breathing cathode for wastewater treatment and simultaneous electricity production. Chem. Eng. J. 253, 174–182.

Kaneko, M., Ueno, H., Saito, R., Yamaguchi, S., Fujii, Y., Nemoto, J., 2009. UV light-activated decomposition/cleaning of concentrated biomass wastes involving also solid suspensions with remarkably high quantum efficiency. Appl. Catal. B 91, 254–261.

Paracchino, A., Laporte, V., Sivula, K., Grätzel, M., Thimsen, E., 2011. Highly active oxide photocathode for photoelectrochemical water reduction. Nat. Mater. 10, 456.

S. Masudy-Panah, R. Siavash Moakhar, C.S. Chua, A. Kushwaha, G.K. Dalapati, Stable and efficient CuO based photocathode through oxygen-rich composition and Au–Pd nanostructure incorporation for solar-hydrogen production, ACS Appl Mater Interfaces 9 (2017) 27596–27606.

S. Masudy-Panah, R. Siavash Moakhar, C.S. Chua, H.R. Tan, T.I. Wong, D. Chi, G.K. Dalapati, Nanocrystal engineering of sputter-grown CuO photocathode for visible-light-driven electrochemical water splitting, ACS Appl. Mater. Interf. 8 (2016) 1206–1213.

Esposito, D.V., Baxter, J.B., John, J., Lewis, N.S., Moffat, T.P., Ogitsu, T., O'Neil, G.D., Pham, T.A., Talin, A.A., Velazquez, J.M., 2015. Methods of photoelectrode characterization with high spatial and temporal resolution. Energy Environ. Sci. 8, 2863–2885.

Mecha, A.C., Onyango, M.S., Ochieng, A., Momba, M.N., 2017. Evaluation of synergy and bacterial regrowth in photocatalytic ozonation disinfection of municipal wastewater. Sci. Total Environ. 601, 626–635.

Liu, J., Bai, H., Wang, Y., Liu, Z., Zhang, X., Sun, D.D., 2010. Self-assembling TiO2 nanorods on large graphene oxide sheets at a two-phase interface and their anti-recombination in photocatalytic applications. Adv. Funct. Mater. 20, 4175–4181.

Neelgund, G.M., Oki, A., Luo, Z., 2014. ZnO and cobalt phthalocyanine hybridized graphene: efficient photocatalysts for degradation of rhodamine B. J. Colloid Interface Sci. 430, 257–264.

Thakur, S., Kshetri, T., Kim, N.H., Lee, J.H., 2017. Sunlight-driven sustainable production of hydrogen peroxide using a CdS–graphene hybrid photocatalyst. J. Catal. 345, 78–86.

Chen, Y., Sun, F., Huang, Z., Chen, H., Zhuang, Z., Pan, Z., Long, J., Gu, F., 2017. Photochemical fabrication of SnO_2 dense layers on reduced graphene oxide sheets for application in photocatalytic degradation of p-nitrophenol. Appl. Catal. B 215, 8–17.

Zang, G.-L., Sheng, G.-P., Shi, C., Wang, Y.-K., Li, W.-W., Yu, H.-Q., 2014. A bio-photoelectrochemical cell with a MoS 3-modified silicon nanowire photocathode for hydrogen and electricity production. Energy Environ. Sci. 7, 3033–3039.

Wang, D., Li, Y., Puma, G.L., Wang, C., Wang, P., Zhang, W., Wang, Q., 2015. Dye-sensitized photoelectrochemical cell on plasmonic Ag/AgCl@ chiral TiO2 nanofibers for treatment of urban wastewater effluents, with simultaneous production of hydrogen and electricity. Appl. Catal. B 168, 25–32.

Zhang, Y., Wang, Y., Angelidaki, I., 2015. Alternate switching between microbial fuel cell and microbial electrolysis cell operation as a new method to control H_2O_2 level in Bioelectro-Fenton system. J. Power Sources 291, 108–116.

Zhuang, L., Zhou, S., Yuan, Y., Liu, M., Wang, Y., 2010. A novel bioelectro-Fenton system for coupling anodic COD removal with cathodic dye degradation. Chem. Eng. J. 163, 160–163.

Fu, L., You, S.-J., Zhang, G.-Q., Yang, F.-L., Fang, X.-H., 2010. Degradation of azo dyes using in-situ Fenton reaction incorporated into H2O2-producing microbial fuel cell. Chem. Eng. J. 160, 164–169.

Thor, S.-H., Ho, L.-N., Ong, S.-A., Nordin, N., Ong, Y.-P., Yap, K.-L., 2020. Explicating the importance of aeration and pH for Amaranth degradation and electricity generation in a viable hybrid system of photocatalytic fuel cell and electro-Fenton process. Sep. Purif. Technol. 239, 116535.

Feng, C., Li, F., Liu, H., Lang, X., Fan, S., 2010. A dual-chamber microbial fuel cell with conductive film-modified anode and cathode and its application for the neutral electro-Fenton process. Electrochim. Acta 55, 2048–2054.

Brillas, E., Sirés, I., Oturan, M.A., 2009. Electro-Fenton process and related electrochemical technologies based on Fenton's reaction chemistry. Chem. Rev. 109, 6570–6631.

Nordin, N., Ho, L.-N., Ong, S.-A., Ibrahim, A.H., Wong, Y.-S., Lee, S.-L., Oon, Y.-S., Oon, Y.-L., 2017. Hybrid system of photocatalytic fuel cell and Fenton process for electricity generation and degradation of Reactive Black 5. Sep. Purif. Technol. 177, 135–141.